PERFORMANCE OF A TWO-STAGE LAUNCHER USING HYDROGEN

By

W. B. Stephenson and R. E. Knapp

von Kármán Gas Dynamics Facility

ARO, Inc.,

a subsidiary of Sverdrup and Parcel, Inc.

March 1962

ARO Project No. 386079

AF - AEDC
Arnold AFS Tenn

ABSTRACT

A procedure is outlined for computing the performance of two-stage, light-gas launchers using hydrogen as a propellant. A method in general dimensionless terms is developed by which the launch velocity for this type of launcher may be computed. The effects of piston weight and velocity, as well as preheating of the pump tube gas, are determined. Experimental results using both unheated and heated hydrogen are compared with theoretical calculations of velocity.

Since the important physical variables -- piston mass, velocity, pump tube geometry, initial pump tube pressure, piston reversal, initial projectile movement, and heat losses -- are included, a design optimization has been made, and limits to the launch velocity have been estimated.

CONTENTS

TABLE

ILLUSTRATIONS

NOMENCLATURE

A	Cross-section area
a	Acoustic speed
C_p	Specific heat at constant pressure
C_v	Specific heat at constant volume
d	Diameter
E	Internal energy
H	Enthalpy
K	Thermal conductivity at temperature T
KE	Kinetic energy
ℓ	Length
m	Mass
P	Pressure
q	Velocity relative to the shock
$\dot{q}$	Heat transfer rate
R	Gas constant
S	Entropy
s	Distance
T	Temperature
t	Time
u	Velocity
u_t	Thermodynamic launch velocity (no chambrage, infinite chamber length)
V	Volume
Z	Compressibility factor
γ	Ratio of specific heats
λ	Empirical factor
μ	Absolute viscosity
ρ	Density

SUBSCRIPTS

c	Chamber
F	Final state in pump tube
g	Pump tube gas
I	Ideal
L	Launch tube
M	Projectile
n	Any number
o	Standard conditions, T_o – 300°K, P_o – 1 atm
p	Piston or pump tube
S	Shock
w	Wall
1	Ahead of incident shock
2	Behind incident shock
3	Behind first reflected shock
4	Behind first shock reflected from piston face

} normal shocks

DIMENSIONAL COORDINATES

$\bar{s}$	$\frac{P_F A_L}{m_M a_F^2} s$
$\bar{t}$	$\frac{P_F A_L}{m_M a_F} t$
$\bar{u}$	u/a_F
$\bar{a}$	a/a_F
$\bar{P}$	P/P_F

P_F, a_F Initial chamber conditions, corresponding to final state in pump tube

m_M Projectile mass

1.0 INTRODUCTION

Helium has been used extensively in light-gas model launcher work because of its chemical inertness, its ease of handling, and the fact that its thermodynamic properties are close to ideal. However, experiments at the Ames Research Center (NASA) and at Arnold Engineering Development Center (AEDC) have demonstrated that appreciably higher launch speeds are attained using hydrogen. The maximum velocity obtained from a typical 0.5-in. launcher was 23,500 ft/sec using helium (Ref. 1); whereas, 29,600 ft/sec was reached when hydrogen was the propellant.

The reason for the failure of helium to provide high velocities became apparent in the process of correlation of experimental results with ideal calculations. For the same maximum pressure, the ideal velocity is about the same for either propellant; however, the gas temperature is much higher for helium. An empirical correction derived in Ref. 1 for the effect of high temperatures is shown in Fig. 1 and demonstrates the relative potential performance of simple launchers consisting of a chamber and launch tube. The lines marked ① are based on an infinitely long chamber having the same bore as the launch tube with a maximum pressure of 300,000 psi. There is a continuous increase in launch velocity with chamber temperature. The introduction of the correction to velocity for temperature leads to maxima of about 21,000 ft/sec for helium and 29,000 for hydrogen (curves ②). If an infinitely large diameter chamber is available to supply the launch tube, these velocities are 26,500 and 37,000 ft/sec (curves ③). As a conceivable ultimate in launch velocity, the pressure might be doubled, the launch tube length doubled, or the projectile mass halved. The result of each of these changes would be about a 15-percent increase in velocity with hydrogen. Actual maximum velocities obtained for a 1/2 caliber plastic projectile are shown. The velocity attained with helium was very near the peak, but evidently further heat addition can be used to advantage with hydrogen. This fact suggests that preheating of hydrogen before compression in the pump tube will be effective. This has been accomplished during the development program, and it was found that a 600°K charge temperature produced about 10 percent average velocity increase over that obtained with 300°K charge temperature.

The method of estimating the performance of a two-stage adiabatic compression launcher was outlined in detail in Ref. 1 for ideal helium. The calculation for hydrogen is essentially the same except that the processes during compression are based on the best available thermodynamic data for the real gas at high pressures. These comprise:

Manuscript released by authors January 1962.

(a) National Bureau of Standards tables in the temperature range from 300 to 600°K and pressures to about 1000 atm, (b) unpublished data from Hilsenrath (NBS) in the regime above 2200°K to 1000 Amagat, which however does not include covolume effects, and (c) a computer program which includes covolume effects but neglects ionization and dissociation for the region between (a) and (b). Appendix A discusses these data in detail.

2.0 IDEAL INTERIOR BALLISTICS

The estimation of pressures and velocities in the two-stage launcher is based on the following simplified models (Fig. 2): (a) the piston has acquired the velocity, u_p, as it nears the end of the pump tube, and its driving pressure is negligible thereafter, (b) the incident shock reflects from the end of the pump tube leaving a state ③ at rest, (c) the shock reflects from the piston face leaving the state ④, (d) the piston comes to rest with the pump tube gas at a final state having the entropy of state ④ and the internal energy of state ③ plus the piston kinetic energy, and (e) the projectile does not move until the final state is attained, after which its motion is determined from the expansion of an ideal gas without friction in an evacuated bore. Figure 3 shows the effect of final pressure and temperature on thermodynamic velocity, u_t. The thermodynamic velocity is determined only by the final state since it is computed for the launch tube supplied from an infinitely long chamber having the same bore. The effect of actual chamber geometry (the volume in the pump tube after compression) is derived from the characteristics method computations of Ref. 2 for helium. Figure 4 shows the effect of chamber geometry on ideal launch velocity, u_I, in terms of thermodynamic velocity, u_t.

The ideal launch velocity is based upon the following simplifications to the actual situation: (1) there are no heat losses from the propellant, (2) the projectile remains stationary until the final pressure is reached, and (3) the piston comes to rest and remains fixed at the final state position. These deviations from the actual case require empirical correction factors derived from a series of experimental firings in a 0.5-in. launcher. The effects are discussed in the following sections.

3.0 EFFECT OF FINAL TEMPERATURE

In Ref. 1 experimental results from a 0.5-in. bore launcher operated with both helium and hydrogen were reported. Final temperatures ranged from 3,000 to over 14,000°K for helium and from 2000 to 3000°K for hydrogen. A comparison of ideal and measured launch velocity showed a very striking effect of final temperature on the velocity attained. The velocity loss was almost linear above a temperature of 2000°K having a magnitude:

$$\frac{\Delta u}{u_I} = -3\,(T_F - 2000°K) \times 10^{-5} \qquad T_F > 2000°K$$

In addition to reducing the propelling energy of the driving gas by heat loss to the wall, high temperatures may cause vaporization of the wall and therefore contamination of the light gas by a heavy element which further reduces the launch velocity. Much greater erosion of launch tubes is evident when helium, rather than hydrogen, is used as a propellant. A simple comparison of the two gases based on laminar flat plate heat transfer may give some insight into the problem of excessive final temperatures. The ratio of heat transfer rates is

$$\frac{\dot{q}_{He}}{\dot{q}_{H_2}} = \left(\frac{\mu_{H_2}}{\mu_{He}}\right)^{1/6}\left(\frac{C_{p_{He}}}{C_{p_{H_2}}}\right)^{1/3}\left(\frac{K_{He}}{K_{H_2}}\right)^{2/3}\left(\frac{T_{H_2}}{T_{He}}\right)^{1/2}\left(\frac{T_{He} - T_w}{T_{H_2} - T_w}\right)$$

If the same heat is added to the two, their temperatures are in the ratio

$$T_{H_2}/T_{He} = \frac{C_{v_{He}}}{C_{v_{H_2}}} \cong .3$$

A typical final temperature for hydrogen is 2500°K; (He temperature ≅ 8300°K) then, as the walls absorb the heat, the relative heat transfer of the gases is indicated in the following table:

T_w, °K	$\dot{q}_{He}/\dot{q}_{H_2}$
300	1.0
1000	1.34
1500	1.93
2000	3.48

At about 1800°K, the melting temperature of the wall is reached. Helium will supply about three times as much heat for melting and vaporization as hydrogen. When gas temperatures exceed 6000-8000°K, radiation becomes a large fraction of the heat loss. A comparison of thermodynamic and ideal velocities is shown in Fig. 1. Distinct maxima occur between 8000 and 10,000°K.

4.0 INITIAL PROJECTILE MOTION

Since the projectile is not restrained in the launch tube after the first shock reflection, its movement before peak pressure is reached would be expected to impair the launcher's performance. The time interval between the first shock arrival and maximum pressure will increase with pump tube length and decrease with piston speed. In addition, the magnitude of the pressure which initially accelerates the projectile increases with both piston speed and initial pump tube charge pressure, p_1. The experimental firings, previously referred to, gave an empirical correction to the ideal launch velocity of the following form*

$$\frac{\Delta u}{u_I} = - 7.4 \, (\Delta s/\ell_L)^3$$

where $\Delta s/\ell_L$ is the fraction of the launch tube traversed in the interval of time between the first and second shock arrivals at the end of the pump tube, assuming constant piston speed. The derivation of this distance follows:

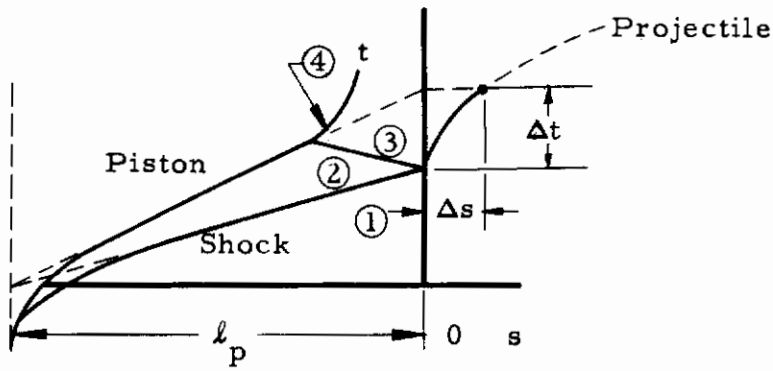

The diagram indicates the shock speeds, u_{s_1}, u_{s_2}, and u_{s_3}: the incident, first reflected, and second reflected shocks. The time interval, Δt, between arrival of the incident and second reflected shocks is:

$$\Delta t = \ell_p \left(1 - \frac{u_p}{u_{s_1}}\right)\left(1 - \frac{u_p}{u_{s_2}}\right)\left(\frac{1}{u_{s_2} - u_p} + \frac{1}{u_{s_3}}\right)$$

or

$$\Delta t = \frac{\ell_p}{a_1} f_{\Delta t}\left(\frac{u_p}{a_1}\right)$$

The distance moved, Δs, is then determined from the dimensionless time-distance relationship (Ref. 1)

$$\Delta s = \frac{m_M \, a_3^2}{P_3 \, A_L} f_{\bar{t}}\left(\frac{P_3 \, A_L}{m_M \, a_3} \Delta t\right)$$

where

$$f_{\bar{t}} = \bar{s} \, (\bar{t}) \qquad \text{(Ref. 2)}$$

*Recent experiments have led to a revision in this correction factor. A correction of the form $\frac{\Delta u}{u_I} = - 0.92 \times 10^{-6} \left(\frac{\Delta s}{d_L}\right)^3$ is suggested.

In dimensionless terms,

$$\frac{\Delta s}{\ell_p} = \frac{m_M a_1^2}{P_1 A_L \ell_p}\left(\frac{P_1}{P_3}\right)\left(\frac{a_3}{a_1}\right)^2 f_{\bar{t}}\left[\frac{P_1 A_L \ell_p}{m_M a_1^2}\left(\frac{a_1}{a_3}\right)\left(\frac{P_3}{P_1}\right) f_{\Delta t}\left(\frac{u_p}{a_1}\right)\right]$$

$$= f\left[\left(\frac{P_1 A_L \ell_p}{m_M a_1^2}\right), \frac{u_p}{a_1}\right]$$

This relation is shown in Fig. 5 for $\gamma = 1.4$, which is considered adequately accurate for the moderate pressures and temperatures of condition (3). The influences of piston speed, pump tube length, and initial pump tube pressure are clearly evident.

5.0 PISTON REVERSAL

A piston reversal parameter of the form $\left(\frac{m_p A_L}{m_M A_p}\right)$ was derived in Ref. 1, which provided a correlation based on a rather limited number of firings with light pistons or heavy projectiles. The form of the correction was tentatively found to be

$$\frac{\Delta u}{u_I} = -\frac{0.4}{\left(\frac{m_p A_L}{m_M A_p}\right)^2}$$

The physical significance of the parameter $\left(\frac{m_p A_L}{m_M A_p}\right)$ is obviously the relative initial accelerations of piston and projectile. For practical high velocity launcher configurations, this correction is usually small (less than 2 percent).

It should be emphasized that the empirical corrections discussed above are not large for high velocity firings when hydrogen is used. The maximum value of the total correction was between four and eight percent for the rounds cited in the section, "Experimental Results," when the launch velocity exceeded 25,000 ft/sec. Therefore, a high degree of exactitude in computing these values is not considered necessary.

6.0 EFFECT OF FINAL VOLUME IN THE PUMP TUBE

The difference between thermodynamic velocity (based on the final state and calculated for a launch tube having no chambrage and infinite chamber length) and the ideal velocity (which incorporates the final geometry of the pump tube gas) is important in proportioning launcher configurations of the two-stage type. In Ref. 2, characteristics method calculations were presented for helium ($\gamma = 1.66$) for several chambrage (A_p/A_L)

values and chamber lengths (see also Refs. 4, 5, and 6). These are summarized in Fig. 4 in the form of the ratio of ideal velocity/thermodynamic velocity for various chamber volume/launch tube volume ratios for constant dimensionless projectile travel values ($\bar{s}$). It is assumed that the effects of chambrage and chamber length practically compensate when chamber volume is fixed. Therefore, the curves labeled $A_p/A_L = 4$ are used in computing ideal velocity.

The validity of Fig. 4 for hydrogen has not been demonstrated rigorously. However, Figs. 6 and 7 lend support to the reasonableness of the assumption. The effect of chambrage for infinitely long chambers is practically independent of γ as shown in Fig. 6. Figure 7 shows that the distance moved by the projectile when it is overtaken by the first reflected characteristic is also only slightly affected by γ.

7.0 PERFORMANCE CALCULATION

The thermodynamic properties for hydrogen were obtained as discussed in Appendix A and used to calculate the normal shock relationships (Fig. B-2) using the method outlined in Appendix B. The launch velocity is determined as follows:

1. Piston Speed

   For an existing launcher, the piston speed may be determined empirically by firing the first stage alone, using a diaphragm at the end of the pump tube to retain the charge pressure. The estimation of piston speed for a H_2-O_2-He combustion driver was treated in Refs. 1 and 3. Figure 8 shows dimensionless piston speed, u_p/a_c, as a function of $\bar{s}$, $\bar{s} = \left(\frac{P_c A_p s_p^*}{m_p a_c^2}\right)$ and $\bar{P}_i = (P_i/P_c)$. Seventy-five and 100-percent combustion curves are shown. This also gives a reasonably accurate estimate of piston speed for a driver in which a powder charge compresses helium. When the piston speed for the combustion driver is to be computed for an experimental firing in which the chamber pressure is measured, a correction to γ and acoustic speed resulting from less than 100-percent combustion must be introduced (Ref. 3).

---

*The piston travel, s_p, may be taken as $0.9\,\ell_p$ to give a reasonable velocity.

2. Shock Compression

The compressibility factor, Z, is read from a plot similar to Fig. A-5. The acoustic velocity, $a_1 = \sqrt{\gamma R T_1 Z_1}$, is then calculated to obtain the piston Mach number. The states of the pump tube gas after the incident shock is reflected from the end of the pump tube (state 3) and after the reflection from the piston (state 4) are given in Figs. B-2a and b.

3. Final State

The simplified model shown in Fig. 2 is used as the basis for graphically finding the final conditions in the pump tube. Since from Fig. A-3 it can be seen that the internal energy of the gas is practically dependent only on temperature, E_3/RT_o and E_4/RT_o can be read from Fig. A-6. E_3/RT_o is then added to the kinetic energy of the piston, $\frac{KE}{m_g RT_o} = \frac{m_p u_p^2 T_1 Z_1}{2P_1 A_p \ell_p T_o}$, at the entropy of state (4) and the final conditions read from Fig. A-3. A more convenient working plot has been developed by plotting E/RT_o vs P in psi for lines of constant S/R (Fig. A-7). The final volume ratio, $V_F/V_1 = \left(\frac{T_F/T_1}{P_F/P_1}\right) Z_F/Z_1$, is then calculated.

4. Thermodynamic Velocity

This velocity assumes no chambrage ($A_L = A_p$) and an infinite chamber length. A dimensionless launch tube length, $\bar{s}_M = \frac{P_F A_L \ell_L}{m_M (a_F)^2}$, is calculated and the thermodynamic velocity, u_t, read from Fig. 3.

5. Ideal Velocity

The ideal velocity includes the effect of chamber geometry by calculating the ratio of final pump tube volume to launch tube volume, $V_F/V_L = V_F/V_1 \times \frac{A_p \ell_p}{A_L \ell_L}$, and using this and $\bar{s}_M$ to read a value of u_t/u_I from Fig. 4.

6. Launch Velocity

The ideal launch velocity is then corrected for the effects of final temperature, piston reversal, and initial projectile motion using the empirical corrections derived in Ref. 1 and discussed in the previous section. The initial projectile

motion is first found by computing the quantity, $P_1 \frac{A_L \ell_p}{m_M (a_1)^2}$,

and using Fig. 5 to get $\Lambda s/\ell_p$, which is then converted to $\Lambda s/\ell_L$. The empirical correction,

$$u_L/u_I = 1 - \left[7.4 \ (\Lambda s/\ell_L)^3 + \frac{.4}{\left(\frac{m_p}{m_M}\frac{A_L}{A_p}\right)^2} + 3 \times 10^{-5}(T_F - 2000)\right],$$

then gives the desired launch velocity, u_L.

8.0 0.5-CALIBER COMBUSTION LAUNCHER PERFORMANCE

In order to investigate the performance of a two-stage launcher, using hydrogen as the pump tube gas, a gun was assembled as shown schematically in Fig. 2. It comprised a combustion driven, 40-mm pump tube 10.5 ft long and a 10-ft, 0.5-in. launch tube. Theoretical calculations of this launcher's performance were carried out for a 1-gram projectile and an 86-gram piston, assuming 100 percent combustion giving a chamber pressure of 20,000 psi. The pump tube charge pressure, P_1, was varied for initial temperatures of 300°K and 600°K, and theoretical launch velocities were calculated as outlined in the preceding section.

Figure 9 indicates that for a given charge pressure, P_1, the final pressure, P_F, is almost independent of the initial temperature, T_1. At 3×10^5 psi final pressure, raising the initial temperature from 300 to 600°K gives an increase in launch velocity of about 2500 ft/sec.

The empirical corrections are shown in Fig. 10. As the pump tube charge pressure, P_1, increases, the final temperature decreases because of the decreasing compression ratio. Conversely, the initial projectile motion increases with P_1 because the pressure, P_3, after shock reflection increases. Increasing initial temperature raises the final temperature and lowers the reflected shock pressure, P_3, and therefore the initial motion.

Figure 11 shows the effect of varying the piston driving pressure while holding the final pressure at 300,000 psi. Increasing chamber pressure requires that the initial pressure be increased also. Since this reduces the compression ratio, the final temperature and therefore the thermodynamic velocity, u_t, decreases with increasing chamber pressure. On the other hand, the final volume increases so that the ideal velocity, u_I, tends to become larger. In the 300°K case a maximum is reached at about 40,000 psi chamber pressure, whereas the heated charge case

still shows an increasing velocity at 45,000 psi. The corrected launch velocity, $u_{l,}$, follows the same trends as the ideal velocity. Approximately a thousand ft/sec increase in launch velocity can be obtained by raising chamber pressure from 20,000 psi to the optimum level or the maximum of about 50,000 psi.

9.0 EXPERIMENTAL RESULTS

The two-stage launcher performance was calculated in the previous section, and a number of rounds were fired at various chamber pressures with several piston weights. An external electric heater provided heated hydrogen to the pump tube. Table 1 summarizes the firing results, and shows the correlation between calculated and experimental launch velocities. Since the chamber diaphragm burst pressure could not be determined exactly, an excess of chamber charge pressure and a slightly higher than the nominal burst pressure were chosen to result in a piston speed close to the nominal value for 100-percent combustion. Up to Round 227, the nominal chamber pressure was 20,000 psi to correspond to Fig. 9. In the later rounds (228-248) chamber pressure and pump tube charge pressure were increased to obtain larger final volumes (Fig. 11). The firings cover a period during which development of the launcher proceeded parallel to derivation of the performance computation method. The latter depended upon assembling good hydrogen thermodynamic data. It was only for the last 25 rounds that the present form of these data was available. Several causes of poor launch velocity were observed: (1) when pistons were too short they sometimes failed to seal high pressures -- Rounds 198-208, (2) the substitution of a lower density Lexan for pistons resulted in greater breakup and occasionally low velocities -- Rounds 214-235, (3) blowout of a transducer in the high pressure section -- Rounds 155, 157, 240, and 242, and (4) apparent failure to attain piston velocity as a result of protective blowout discs in the heater system -- Rounds 202-211 (check valves were installed at the pump tube after 211). Some of the scatter in the data with the heater resulted from the difficulty in setting the highly transient pressure and temperature during these firings.

The measurement of velocity was made with a Beckman-Whitley Model 192 framing camera to better than one percent accuracy except as noted. In these cases where the camera failed, velocity was obtained from two shadowgraph stations 45 ft apart, radiation detectors, or break wires with as much as two or three percent variation. Chamber pressure was measured by Norwood pressure transducers to approximately ±1000 psi.

Figure 12 shows the comparison of measured with calculated launch velocities. These were within five or six percent except for rounds where the difficulties noted above led to low experimental velocities and in four rounds that were excessively high. There are two possible explanations for these rounds. The uncertainties in pump tube charge pressure, chamber pressure, and thermodynamic data combined to lead to a low calculated velocity. Or the calculation is pessimistic in using ideal gas characteristics for the isentropic expansion behind the projectile. During the expansion from the equilibrium state after compression in the pump tube to the rarefied state when high projectile velocities are attained, the compressibility factor, Z, is 5 to 20 percent greater than unity (Fig. A-5). Here the acoustic speed and therefore the propelling force would be larger than given by the ideal gas assumption.

One of the purposes of the experimental program was to verify the effectiveness of preheating the propellant to obtain higher velocity at the same pressure. Theoretical estimates (Fig. 9) showed about 2500 ft/sec would result from doubling the initial temperature at an upper pressure limit of 3×10^5 psi. Figure 12 shows that approximately this improvement in velocity was obtained. There is considerable scatter in the data because final pressure was not maintained at the above level because of the difficulty of exercising close control over chamber pressure and the desire to avoid exceeding the high pressure section structural strength limit.

The launcher tested was not an optimum geometrical configuration. The calculations showed that the small diameter of the pump tube resulted in insufficient final volume for the launch tube. The ratio of ideal to thermodynamic velocity was only slightly greater than one instead of 1.1 to 1.12, which would result if the final volume were increased from ten percent to 40 percent of the launch tube volume. If the diameter of the pump tube doubled, the launch velocity could be increased more than ten percent.

It can be concluded that the method of calculation provides a good estimate of performance of this type of launch system. The empirical corrections are from four to eight percent for the higher velocities. It appears that all the important physical variables have been considered. The effect of preheating the propellant can be realized as a method of improving performance without an increase in maximum pressure.

10.0 GENERAL LAUNCHER PERFORMANCE

Since a method of estimating the launch velocity has been developed which appears to include the important physical variables, it is reasonable to investigate the effects of geometry on performance. The effects of varying launcher geometry can be studied by fixing the launch tube and projectile, then varying the pump tube geometry. A 200-caliber launch tube is selected for a 1-caliber length plastic projectile (sp. gr. 1.2) to represent a reasonable figure for launching aerodynamic models. Pump tube lengths from 0.5 to 2.0 times the launch tube length and diameters from 2.5 to 10 times that of the launch tube are considered. A minimum weight piston is chosen as 1-caliber length plastic which conforms to experience as a lower limit for structural integrity. The final pressure is taken as 300,000 psi to be within reasonable design practice.

The calculation procedure used for finding the launch velocity here is the same as that discussed earlier, with the exception that now the final pressure in the pump tube is fixed. (P_F = 300,000 psi) and the initial conditions are found. Examination of the dimensionless kinetic energy term, $\frac{KE}{m_g R T_o} = \left(\frac{u_p^2}{2}\right)\left(\frac{m_p}{A_p \ell_p}\right)\left(\frac{(T_1/T_0) Z_1}{P_1}\right)$ shows that piston speed, u_p, and the piston mass per unit pump tube volume are sufficient to determine the final state if the initial temperature is fixed.

The results of these calculations are shown in Figs. 13, 14, 15, and 16.

For the minimum mass piston ($m_p = \rho_p A_p d_p$) therefore:

$$\frac{m_p}{A_p \ell_p} = \frac{1.2}{\left(\frac{\ell_p}{d_p}\right)}$$

when

$$\rho_p = 1.2 \text{ gm/cc}$$

High length-diameter ratio and low piston speeds lead to high final temperatures and thermodynamic velocity. This combination tends toward low final volume after compression, however, tending to reduce the ideal launch velocity.

The empirical corrections are affected in the following manner. With large length/diameter ratios or low piston velocity the final temperature correction increases. The initial projectile motion increases with pump tube length, with a decrease in piston speed (Fig. 5), and with decreasing ℓ_p/d_p or P_1 (Fig. 13). The piston reversal effect becomes smaller as the ratio of pump tube to launch tube diameter increases.

These interacting effects on launch velocity are more clearly shown in Fig. 17. Figure 17a shows the thermodynamic velocity which increases with length/diameter ratio of the pump tube and decreases with piston speed. The ranges of the variables were chosen to give near maximum actual launch velocity. In Fig. 17b the ideal velocity shows a reversal of the trends observed in Fig. 17a resulting from the variation of volume left in the pump tube. An exception is the case of the pump tube 10 times the diameter of the launch tube in which the final volume is so large that further increase is ineffective. The ideal velocity decreases with increasing length after reaching a peak because of the effect of ℓ_p/d_p on final volume.

The corrected launch velocity generally follows the trends of the ideal velocity (Fig. 17c). The piston reversal affects the small diameter pump by about 6 percent and becomes negligible for the largest diameter. The initial projectile motion increases with pump tube length and piston speed because the latter requires higher charge pressure, P_1, and therefore a higher first reflected shock overpressure. Final temperature corrections increase with pump tube length and decrease with diameter, as may be seen in Fig. 14. The overall result of the corrections is to reduce the spread resulting from piston speed. This is particularly evident for the pump tube which is 5 launch tube diameters, where the initial projectile motion effect causes the 7000-ft/sec piston speed curve to fall below the other two. The upper limits in piston speed are compatible with driving pressures of a practical level and the pump tube length/diameter ratios.

The following conclusions may be drawn from Fig. 17c:

1. The launch velocity varies only slightly over a wide range of pump tube lengths.
2. For pump tubes having diameters less than 5 launch tube calibers, increasing piston speed has the effect of increasing launch velocity appreciably.
3. There is only about a 6-percent increase in velocity when the pump tube diameter is increased from 5 to 10 launch tube diameters.

It appears that reasonable configurations of this type of launcher are limited to from 25,000 to 27,000 ft/sec in launching a 1-caliber plastic projectile from a 200-caliber launch tube with unheated hydrogen. As mentioned in the section discussing experimental results, this may be a few percent conservative because of non-ideal isentropic expansion behind the projectile.

An estimate of maximum velocity for the lightest practical projectile (1/2 caliber long) and a launch tube of 300 calibers may be easily made by scaling the above figures by the amount the ideal velocity would be increased. The dimensionless launch tube length ($\bar{s}$) would be increased by 3 and the ratio of final volume in the pump tube to volume of the launch tube decreased by 2/3. This would yield a maximum corresponding to Fig. 17c of about 32,000 ft/sec compared to 27,000 ft/sec. Slightly higher velocities will result from increasing final pressure, but it is difficult to determine structural limits for the projectile or launcher much above the levels used here.

The only appreciable gain in launch velocity appears to result from preheating the charge in the pump tube as has been discussed. The empirical correction for final temperature indicates that temperatures up to about 10,000°K would result in increasing launch velocity (Fig. 1). As a first approximation, the thermodynamic velocity might be taken as a measure of this effect. If 25,300 ft/sec is taken to correspond to the more reasonable pump tube length of 1.5 times launch tube length and 5 times its diameter, this maximum amount of heating would produce a velocity of 31,000 ft/sec. The initial temperature would be around 4000°K for the hydrogen in the pump tube. This is a formidable problem in equipment design whose solution is not yet evident.

11.0 CONCLUSIONS

1. The performance is estimated for two-stage, light-gas, model launchers which utilize an adiabatic compressor in which kinetic energy stored in the piston provides the work of compression.
2. Experimental results indicate that the important physical variables have been included in the proper manner. A moderate amount of preheating of the propellant has been successfully used to increase launch velocity.
3. A systematic study of the effect of varying launcher geometry shows that the limit launch velocity for this type of launcher will not greatly exceed the 30,000-32,000-ft/sec level presently accomplished for unheated hydrogen.
4. The most promising method of raising launch velocity to the 30,000 to 40,000-ft/sec range is by preheating the propellant in the pump tube.

ACKNOWLEDGMENT

The experimental work quoted was under the direction of D. E. Anderson.

REFERENCES

1. Stephenson, W. B. and Anderson, D. E. "Design of a Large, Two-Stage, Light-Gas Model Launcher." AEDC-TR-61-6, June 1961.

2. Stephenson, W. B. "Theoretical Light-Gas Gun Performance." AEDC-TR-61-1, May 1961.

3. Lord, M. E. "Performance of a 40-mm Combustion-Heated, Light-Gas Gun Launcher." AEDC-TN-60-176, October 1960.

4. Courant, R. and Friedrichs, K. O. Supersonic Flow and Shock Waves. Interscience Publishers, Inc., New York, 1948.

5. Seigal, A. E. "The Influence of Chamber Diameter Size on the Muzzle Velocity of a Gun with Effectively an Infinite Length Chamber." NAVORD Report 3635, January 1954.

6. Heybey, W. "A Solution of La Grange's Problem of Interior Ballistics by Means of Its Characteristic Lines." NOL Memorandum 10819, March 1950.

7. Woolley, H. W., Scott, R. B., and Brickwedde, F. G. "Compilation of Thermal Properties of Hydrogen in Its Various Isotopic and Ortho-Para Modifications." NBS Journal of Research, Vol. 41, 1948, pp. 379-475.

8. Hilsenrath, Joseph, et. al. "Tables of Thermal Properties of Gases." NBS Circular 564, 1955, pp. 254-296.

9. Hilsenrath, Joseph. "Unpublished Data on Hydrogen for 2200°K to 18,000°K and Densities to 1000 Amagats."

10. Bjork, R. L. "The Atomic-Hydrogen Gun." RM-1707, July 5, 1961.

11. Stollery, J. L. and Maull, D. J. "A Note on the Compression of Air through Repeated Shock Waves." Journal of Fluid Mechanics, Vol. 4, Part 6, p. 650, November 1958.

12. Lukasiewicz, J., Stephenson, W. B., Clemens, P. L., and Anderson, D. E. "Development of Hypervelocity Range Techniques at Arnold Engineering Development Center." AEDC-TR-61-9, June 1961.

13. Crozier, W. D. and Hume, W. "High Velocity Light Gas Gun." Journal Applied Physics, Vol. 28, No. 8, August 1957.

14. Charters, A. C., Denardo, B. P., and Rossow, Vernon J. "Development of a Piston-Compressor Type Light-Gas Gun for the Launching of Free-Flight Models at High Velocity." NACA TN 4143, November 1957.

15. Bioletti, C. and Cunningham, B. E. "A High Velocity Gun Employing a Shock Compressed Light Gas." NASA TN D-307, February 1960.

TABLE 1
EXPERIMENTAL FIRINGS OF 0.5-IN. LAUNCHER USING HYDROGEN

Round Number	Chamber Pressure	m_p	P_1	m_M	ℓ_L	T_1	$P_{F_{calc}}$	$u_{L_{calc}}$	$u_{L_{exp}}$	$\frac{u_{exp}}{u_{calc}}$	Remarks
	psi	gm		gm	ft	°K	psi	ft/sec	ft/sec		
153	21,100	88 Mic	300	1.00	8.77	300	460,000	26,400	~26,000*	0.98	
154	18,600	88 Mic	450	1.0	8.33	↓	165,000	21,900	18,100	0.83	Barrel Liner Blew Out. Ethocel Transition
155	22,600	87	450	1.0	10.08	↓	260,000	26,200	22,400	0.86	Transducer Blew out of HP Section
157	24,600	82	450	1.0	8.89	↓	222,000	24,300	25,380	1.04	Transducer Blew out of HP Section
158	21,600	78	450	1.0	8.89	↓	205,000	24,600	26,700	1.08	
159	21,000	89 Mic	450	1.0	8.89	↓	230,000	24,600	26,000	1.06	
194	26,000	87	450	1.5	10.25	↓	332,000	26,000	24,500	0.94	
195	25,000	87	425	1.5	10.25	↓	340,000	26,100	18,800	0.72	Low P_F
196	26,000	87	425	1.5	10.25	↓	290,000	25,500	23,900	0.94	
198	22,100	48	400	1.0	9.65	↓	116,000	22,900	22,900	1.00	
199	21,800	48	400	↓	↓	↓	110,000	22,500	19,700*	0.88	Piston Disintegrated. Velocity from oscilloscope
200	24,300	54	425	↓	↓	↓	150,000	24,300	21,900	0.90	
201	22,300	53	425	↓	↓	↓	131,000	23,200	22,000*	0.95	
202	23,000	↓	425	↓	↓	↓	143,000	23,700	22,400*	0.95	Heater Installed. Blow-out Discs in Pump Tube
203	20,000 Est.	↓	450	↓	↓	~600	103,000	24,400	19,500*	0.80	Blow-out Discs
204	23,300	↓	590	↓	↓	~600	94,000	24,000	17,500*	0.73	Low P_F. Blow-out Discs
205	24,300	↓	425	↓	↓	300	150,000	24,200	21,200	0.88	Low P_F. Blow-out Discs
206	23,800	↓	425	↓	↓	↓	117,000	23,300	22,300	0.96	Heater Inlets Plugged.
207	21,800	72 FG	470	↓	↓	↓	165,000	23,900	~22,000	0.92	Heater Inlets Plugged. FG Piston
208	21,000	69 FG	490	↓	↓	↓	148,000	23,400	22,000*	0.94	Heater Inlets Plugged. No Oscillograph Trace, FG Piston
209	25,500	54	455	↓	↓	↓	159,000	24,500	23,000	0.94	P_1 Questionable
210	21,500	53	475	↓	↓	600	110,000	24,800	23,800*	0.96	
211	22,500	86	645	↓	11.00	600	145,000	26,100	25,200*	0.97	
212	22,600	86	670	↓	↓	600	139,000	25,900	26,300	1.02	Inlet Check Valve Downrange End of Pump Tube. Light Lexan Piston
213	24,800	85	655	↓	↓	600	174,000	27,700	26,500	0.96	Eliminated Uprange Blow-out Disc in Pump Tube. P_1 Questionable
214	22,800	86	465	1.08	↓	300	240,000	26,200	29,200	1.11	Light Lexan Piston
215	22,800	↓	465	1.08	↓	300	240,000	26,200	29,200	1.11	Heater Checks Showed Deposite of Fe in Pump Tube
216	22,000	↓	625	1.08	↓	600	145,000	26,100	27,600	1.06	
218	25,500 Est.	↓	530	1.08	↓	650	244,000	29,600	25,500*	0.86	SS Heater Installed. P_1 and Chamber Pressure Questionable
219	21,700	↓	451	1.07	10.87	300	233,000	26,000	26,700*	1.03	
220	24,000	↓	635	1.09	10.87	615	170,000	27,300	25,600	0.94	
221	21,500	↓	655	1.08	10.87	575	129,000	25,100	25,800*	1.03	
223	20,600	80	500	1.04	11.0	300	165,000	23,900	24,700	1.03	Light Lexan Piston This and Following
224	20,800	86	480	1.02	11.0	300	190,000	25,000	26,500	1.06	
225	22,800	87	465	1.11	10.83	300	240,000	27,200	26,100	0.96	
226	21,300	86	550	1.11	↓	575	160,000	26,700	27,000	1.01	
227	21,800	87	530	1.08	↓	575	142,000	26,100	25,500*	0.98	
228	27,800	86	705	1.02	↓	575	132,000	26,000	26,500	1.02	Thermocouple Failed to Retract
229	27,300	86	790	1.00	↓	580	144,000	25,500	20,800*	0.82	Projectile Broke
230	25,800	87	580	1.01	↓	500	188,000	27,400	26,600	0.97	Piston through Launch Tube
231	26,500	↓	715	1.02	↓	615	148,000	26,800	25,500	0.95	Piston through Launch Tube
232	22,300	↓	710	1.01	↓	610	119,000	25,400	23,500	0.93	Piston Sealed but Badly Shattered
233	22,800	↓	610	1.10	↓	300	168,000	23,700	24,600	1.04	Piston through Launch Tube
234	20,000	↓	550	1.11	↓	370	155,000	24,200	25,600	1.06	1/3 Piston through Launch Tube. P_1 not on Oscilloscope Trace
235	23,800	↓	575	1.10	↓	399	184,000	25,800	26,200	1.02	Piston through Launch Tube
236	22,800	↓	688	1.11	↓	430	129,000	24,000	25,000	1.04	Dense Lexan Piston on This and Following. Piston Sealed
237	20,800	86	606	1.09	↓	506	109,000	23,800	26,500	1.11	
238	21,300	↓	597	1.10	↓	606	142,000	25,900	27,300	1.05	
239	20,800	↓	640	1.00	↓	606	117,000	23,900	27,800	1.16	
240	28,300	↓	581	1.00	↓	631	226,000	29,400	27,700	0.94	Blew Plug from HP Section
241	29,400	↓	692	1.09	↓	542	185,000	27,000	26,300	0.97	Thermocouple Failed to Retract
242	32,900	80 FG	575	1.12	↓	666	235,000	29,500	26,200	0.89	FG Piston This and Following Rounds. Plug Blew from HP Section
243	27,000	93 FG	699	1.12	↓	510	160,000	25,800	27,450	1.06	T_1 May Be Higher Than Recorded
244	30,200	97 FG	671	1.13	↓	588	240,000	28,900	28,300	0.98	
245	28,900	97 FG	581	1.12	↓	625	270,000	29,900	28,800*	0.96	
246	28,700	97 FG	555	1.12	↓	590	276,000	29,500	29,600	1.00	T_1 May Be Less Than Recorded
248	30,200	95 FG	530	1.14	↓	710	209,000	29,700	29,300	0.99	

* No Beckman-Whitley Camera Record

Mic Micarta
FG Fiberglass

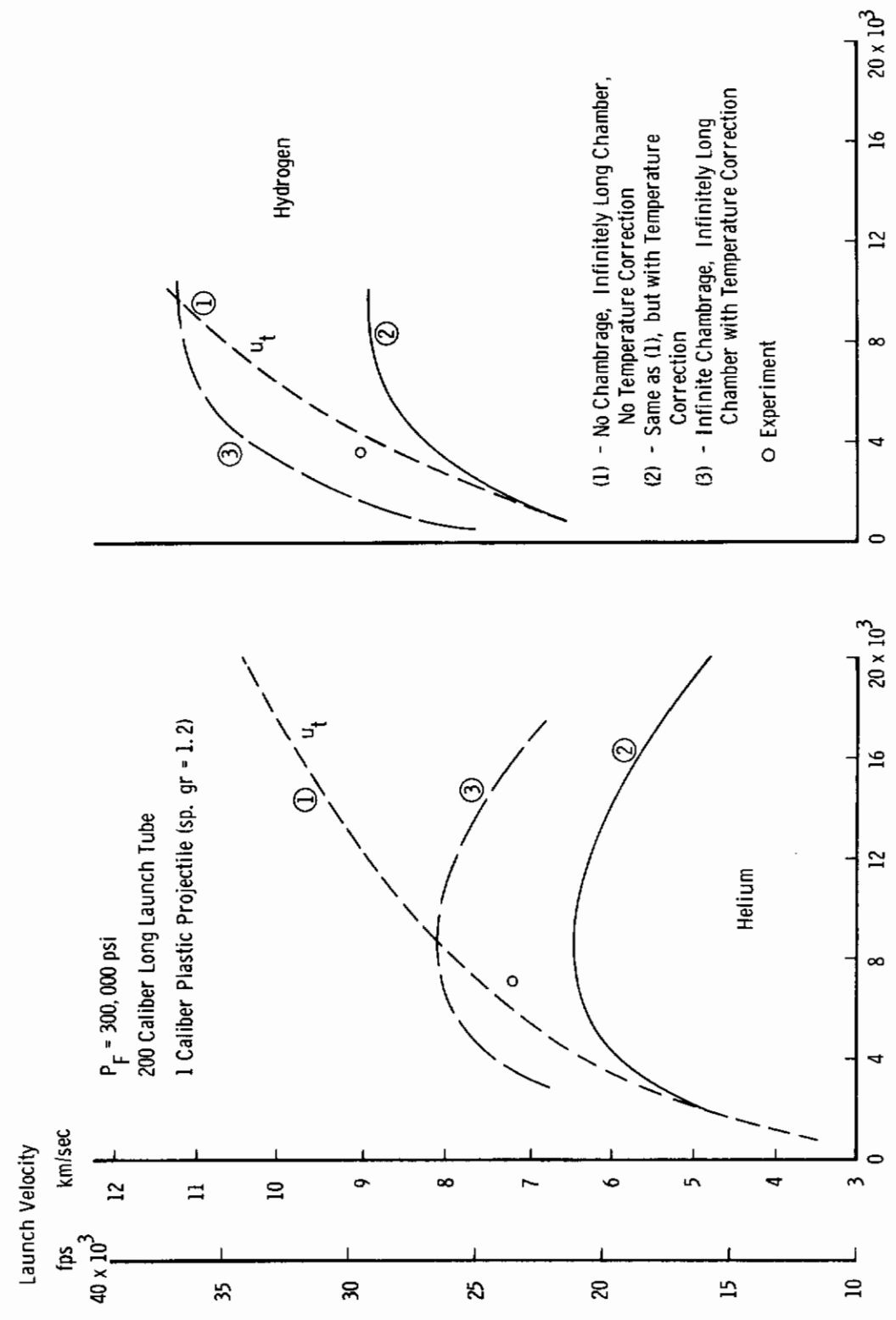

Fig. 1 Effect of Final Temperature on Potential Launch Velocity

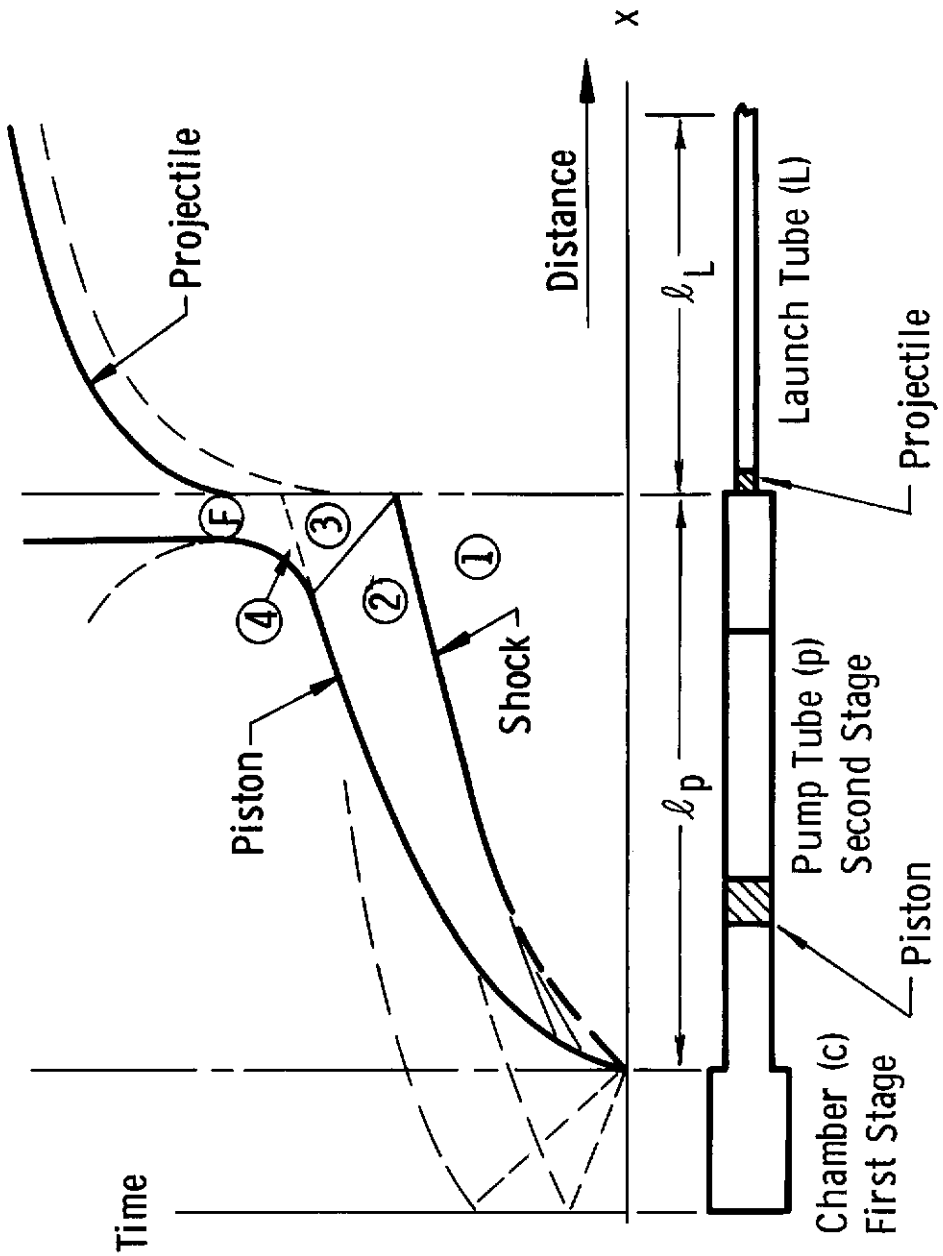

Fig. 2 Launcher Schematic and Distance-Time Diagram

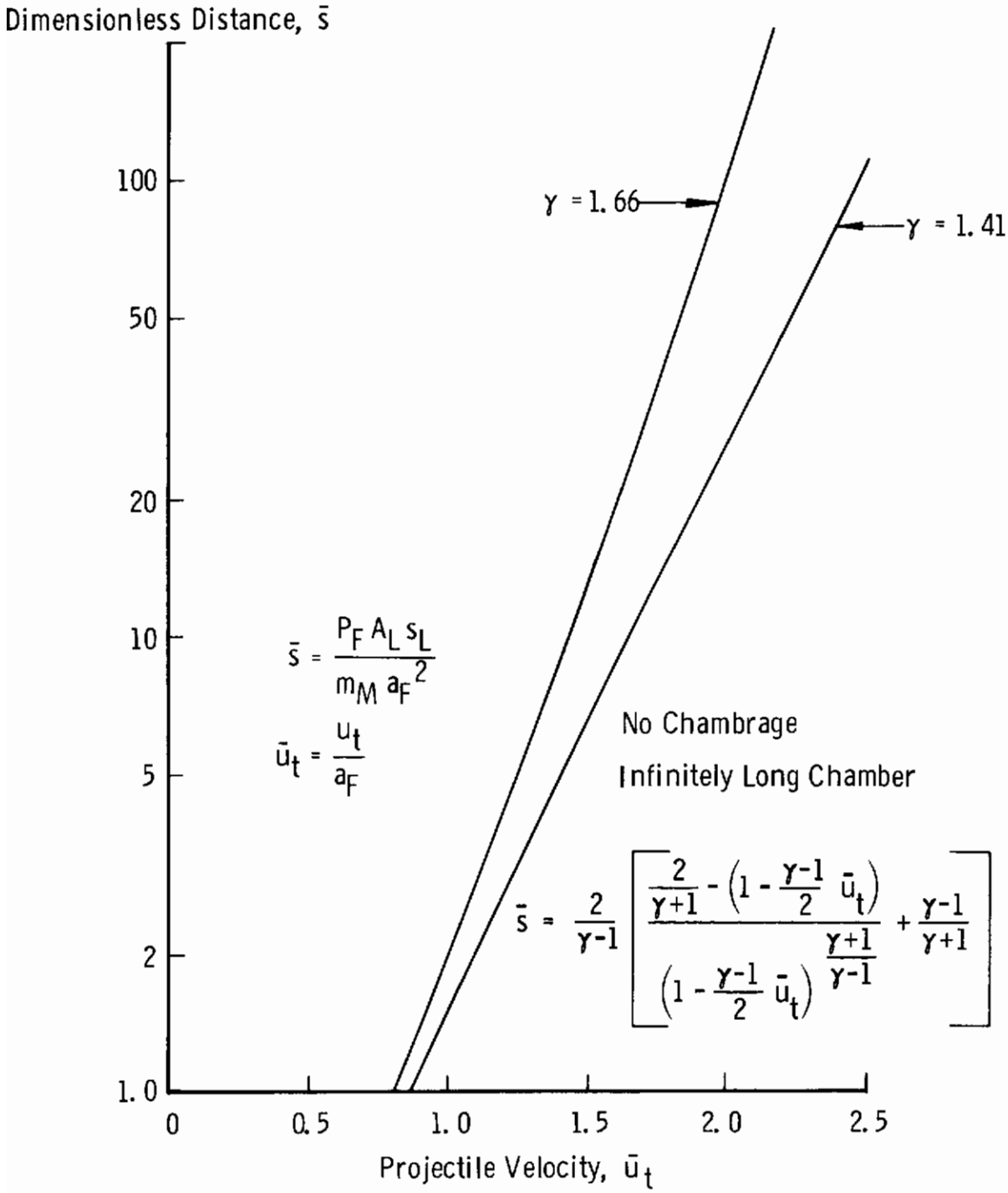

Fig. 3 Dimensionless Projectile Thermodynamic Velocity

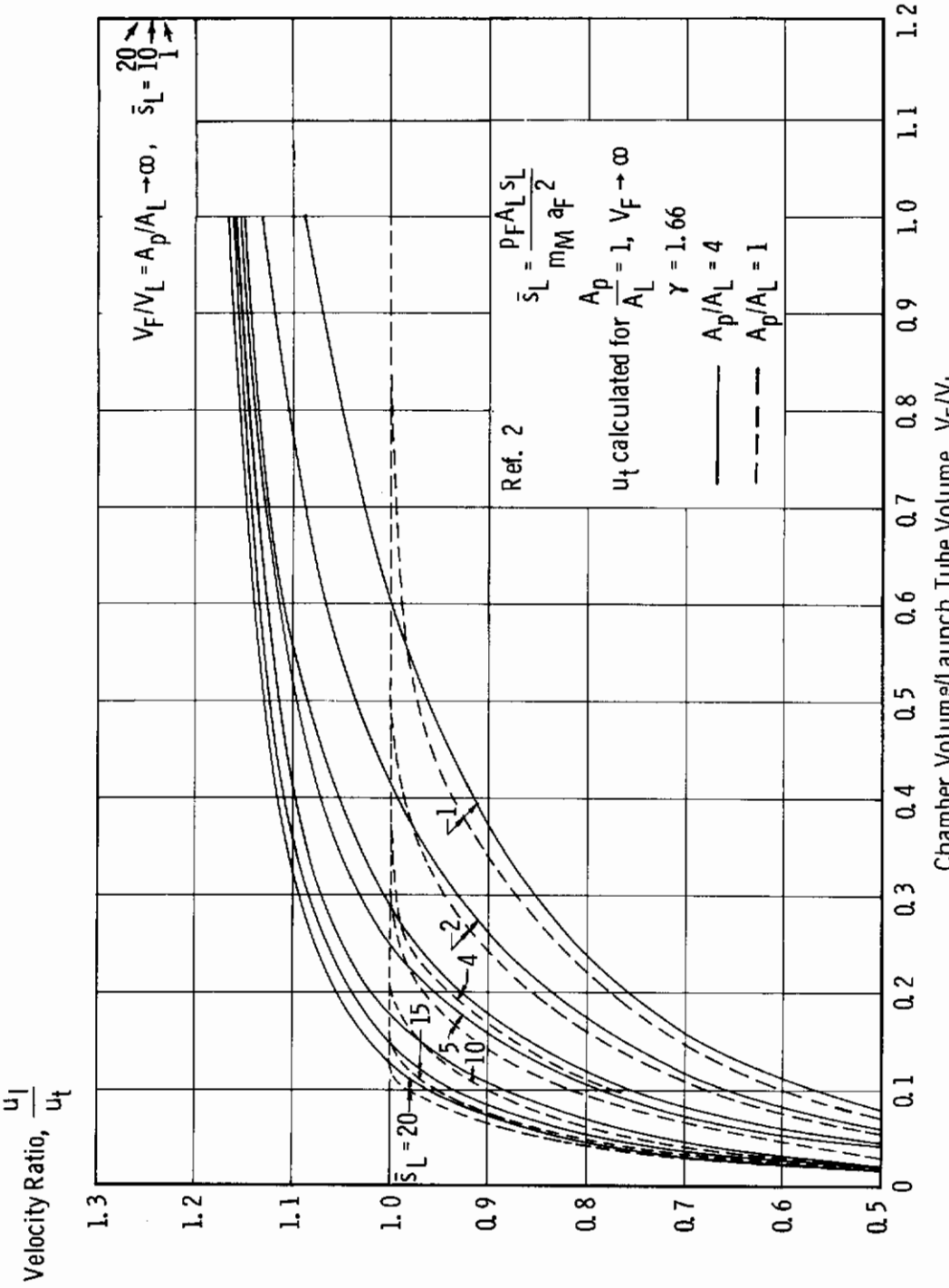

Fig. 4 Effect of Chamber/Launch Tube Volume Ratio on Launch Velocity

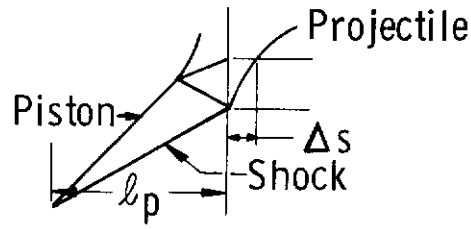

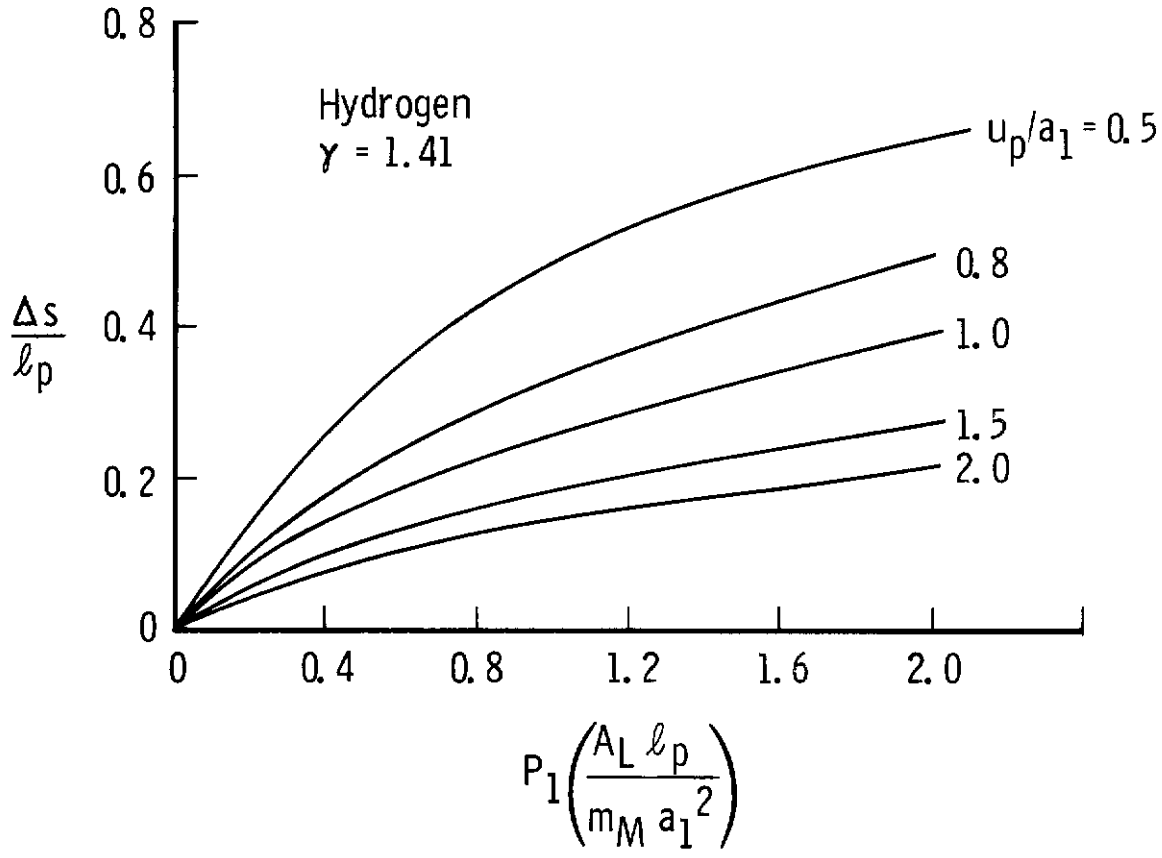

Fig. 5 Initial Projectile Movement

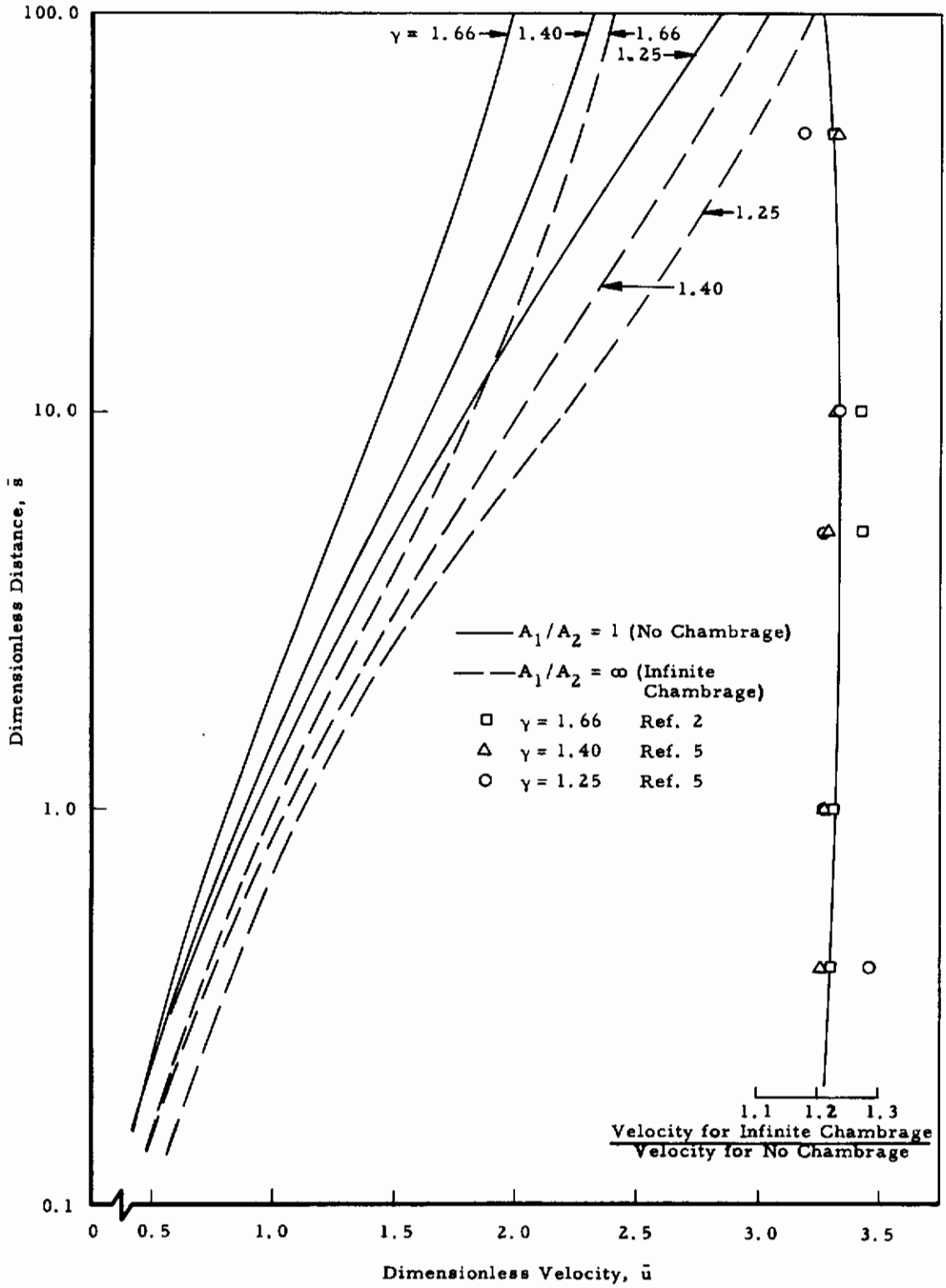

Fig. 6 Effect of γ on Dimensionless Launch Velocity-Distance Relationship

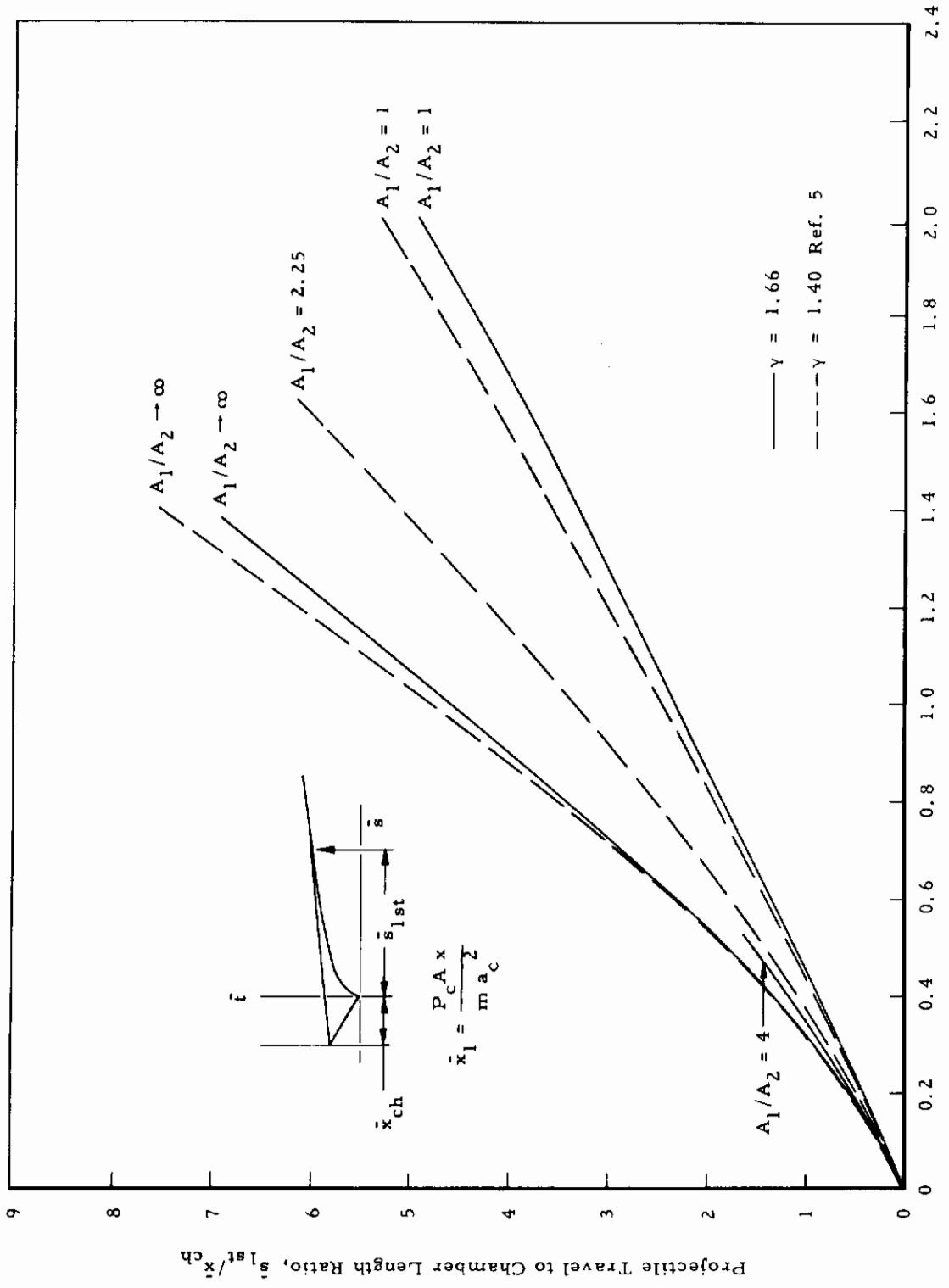

Fig. 7 Projectile Travel When Overtaken by First Reflected Characteristic

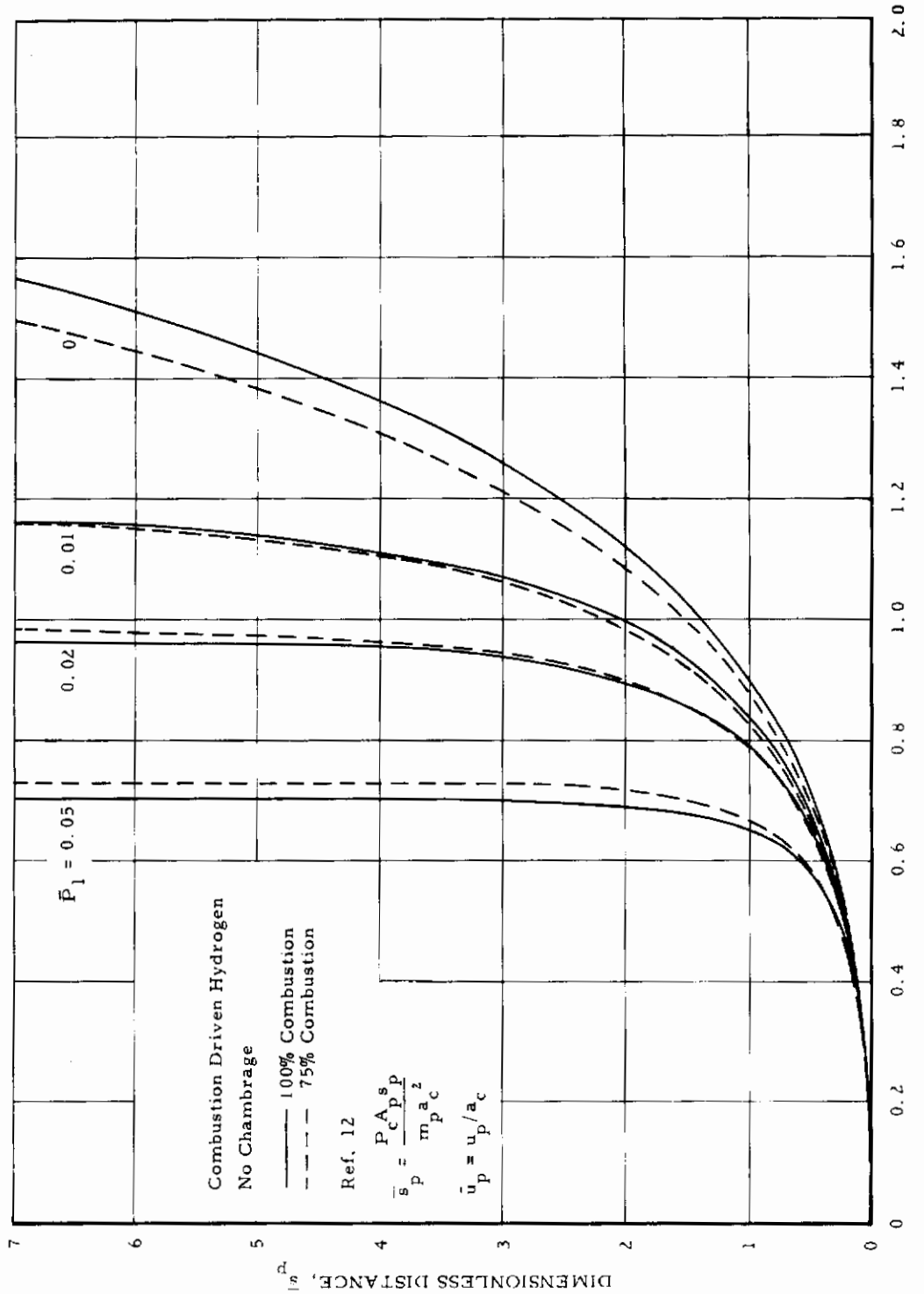

Fig. 8 Dimensionless Piston Speed for H_2-O_2-He Driver

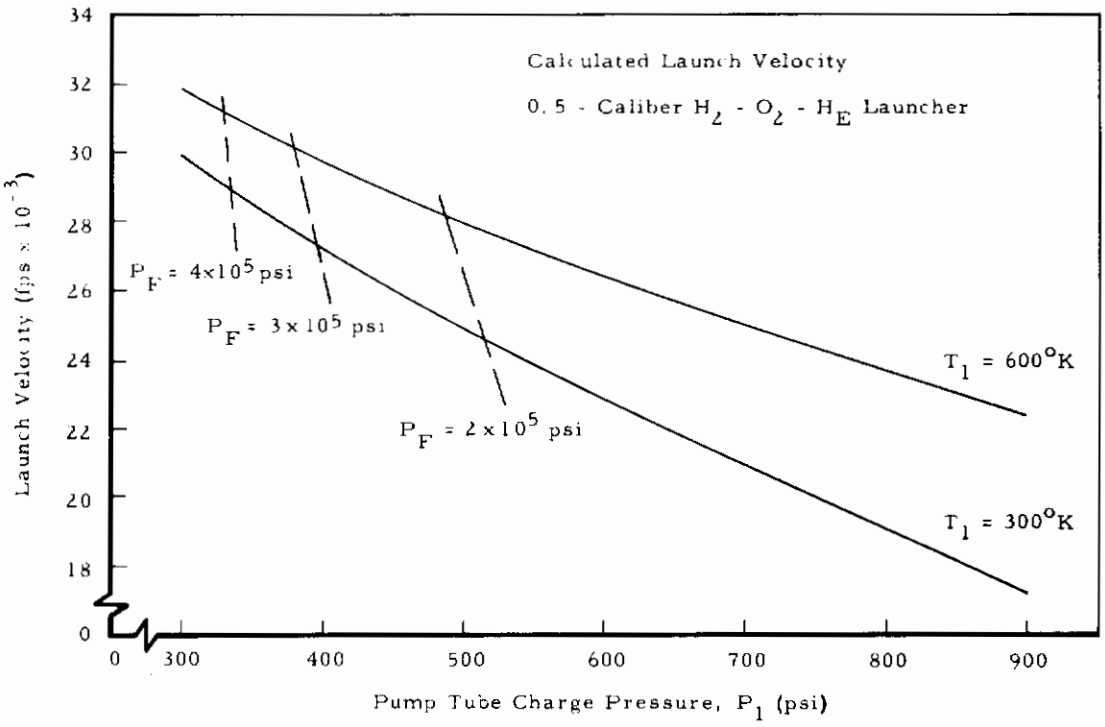

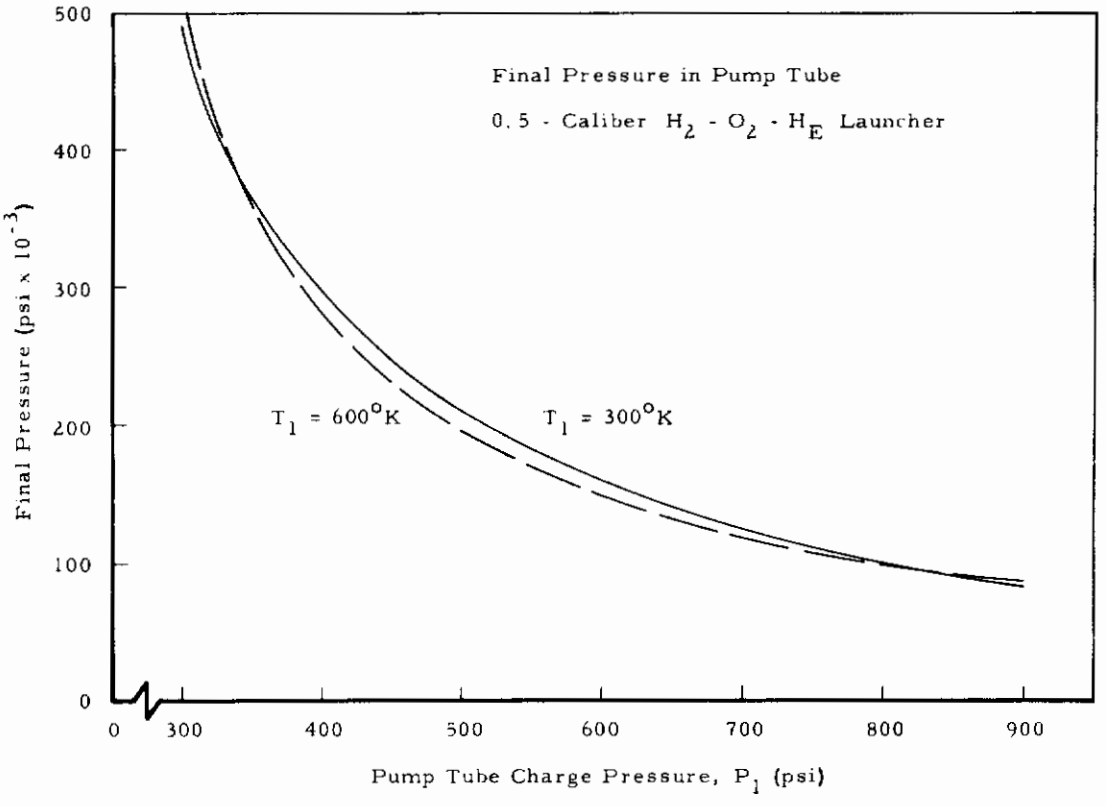

Fig. 9 Calculated Performance of 0.5-Caliber Combustion Driven Launcher

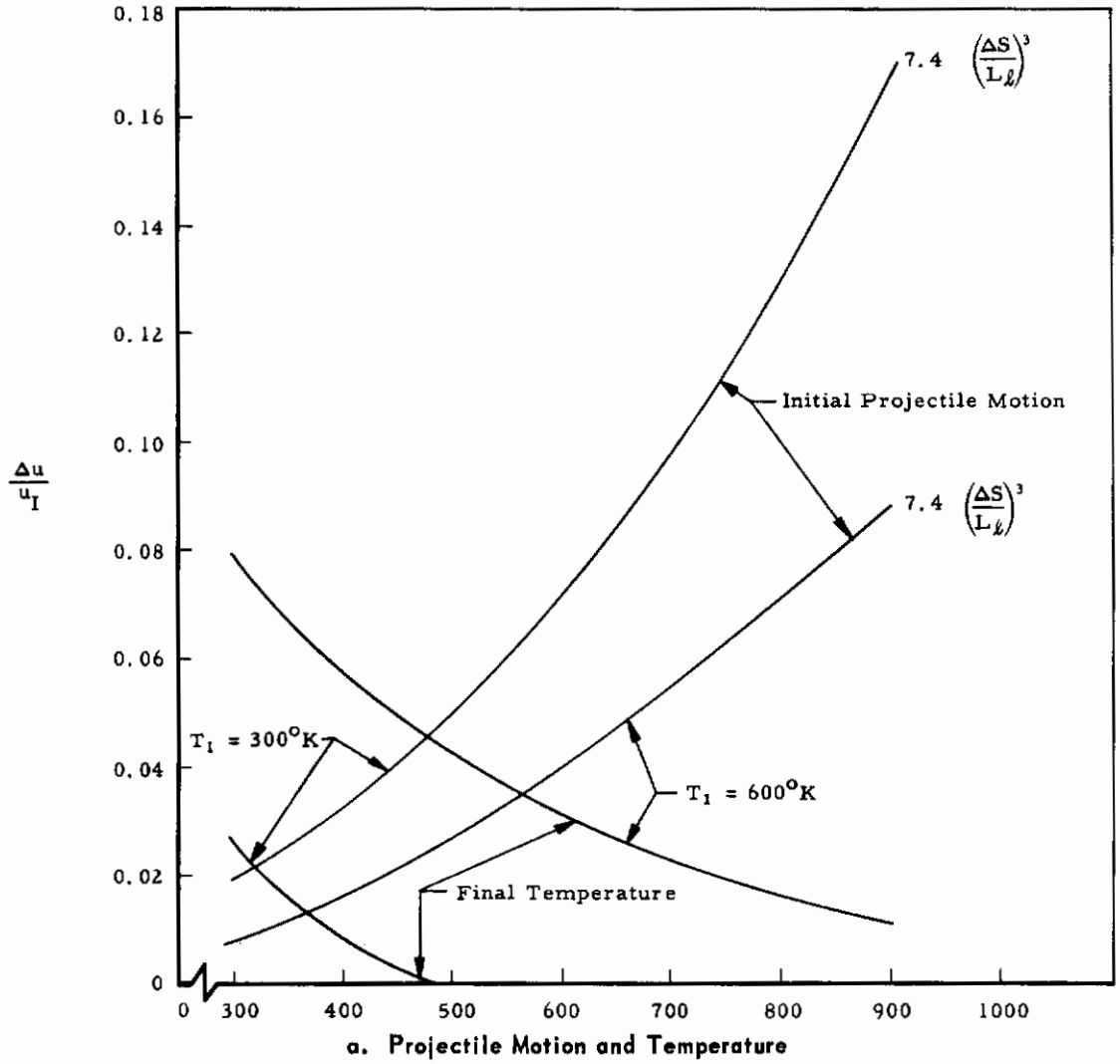

a. Projectile Motion and Temperature

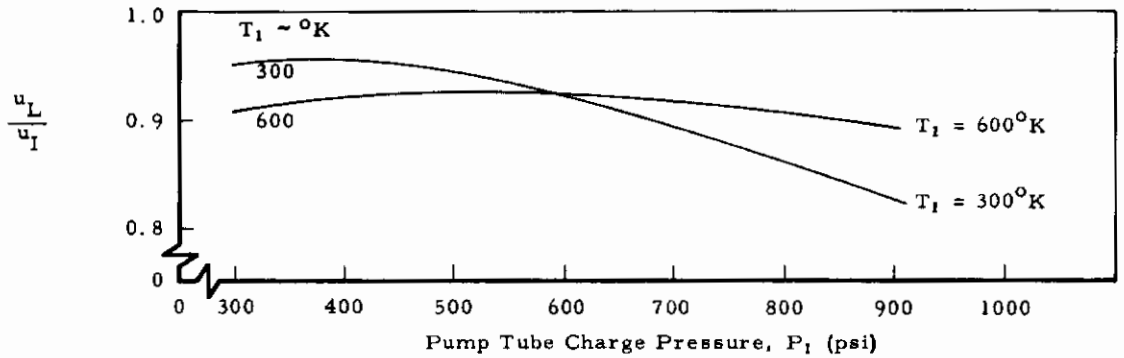

b. Ratio of Launch to Ideal Velocity

Fig. 10 Empirical Corrections to Launch Velocity, 0.5-Caliber Combustion Launcher

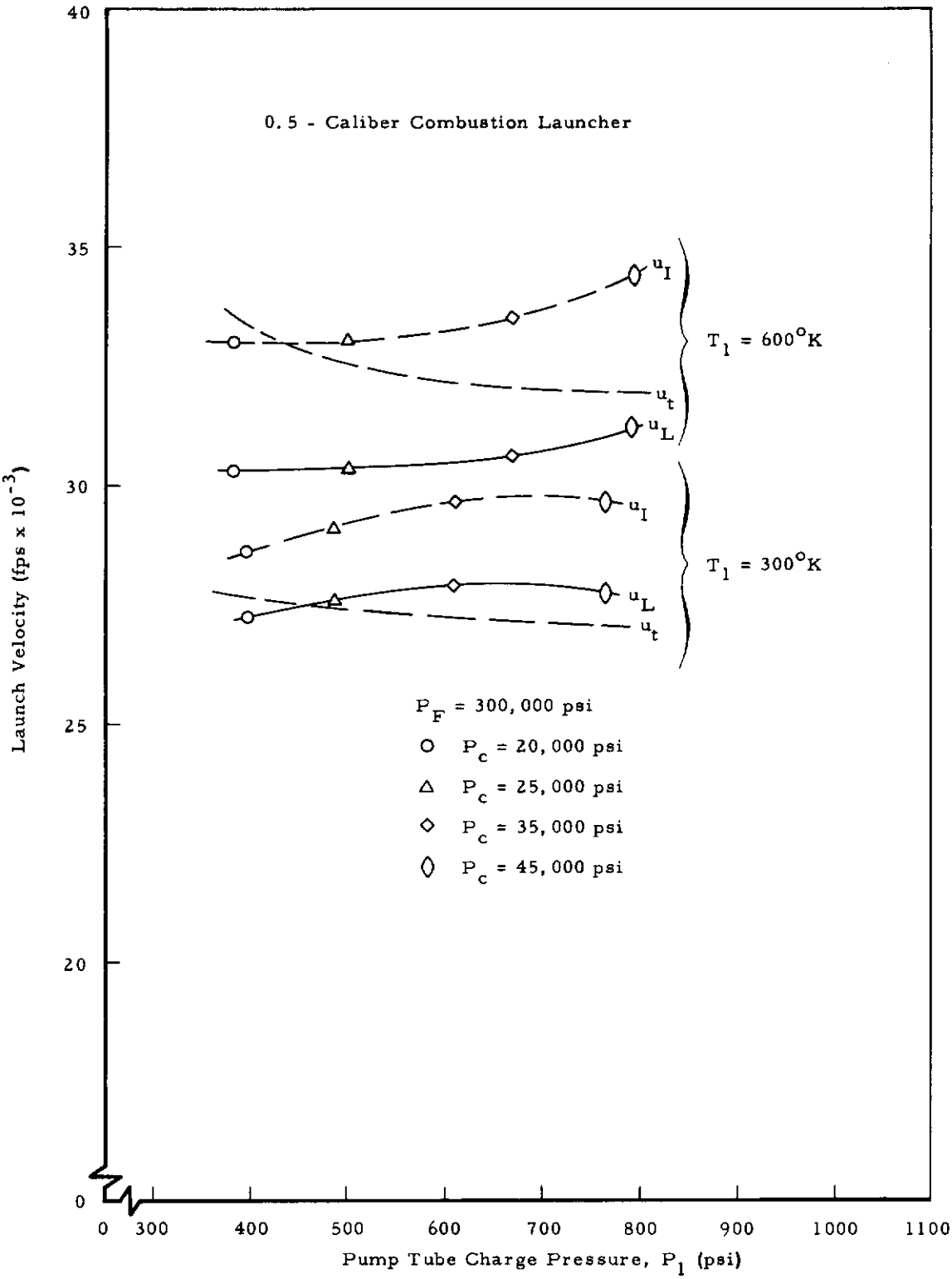

Fig. 11 Effect of Chamber Pressure on Launch Velocity

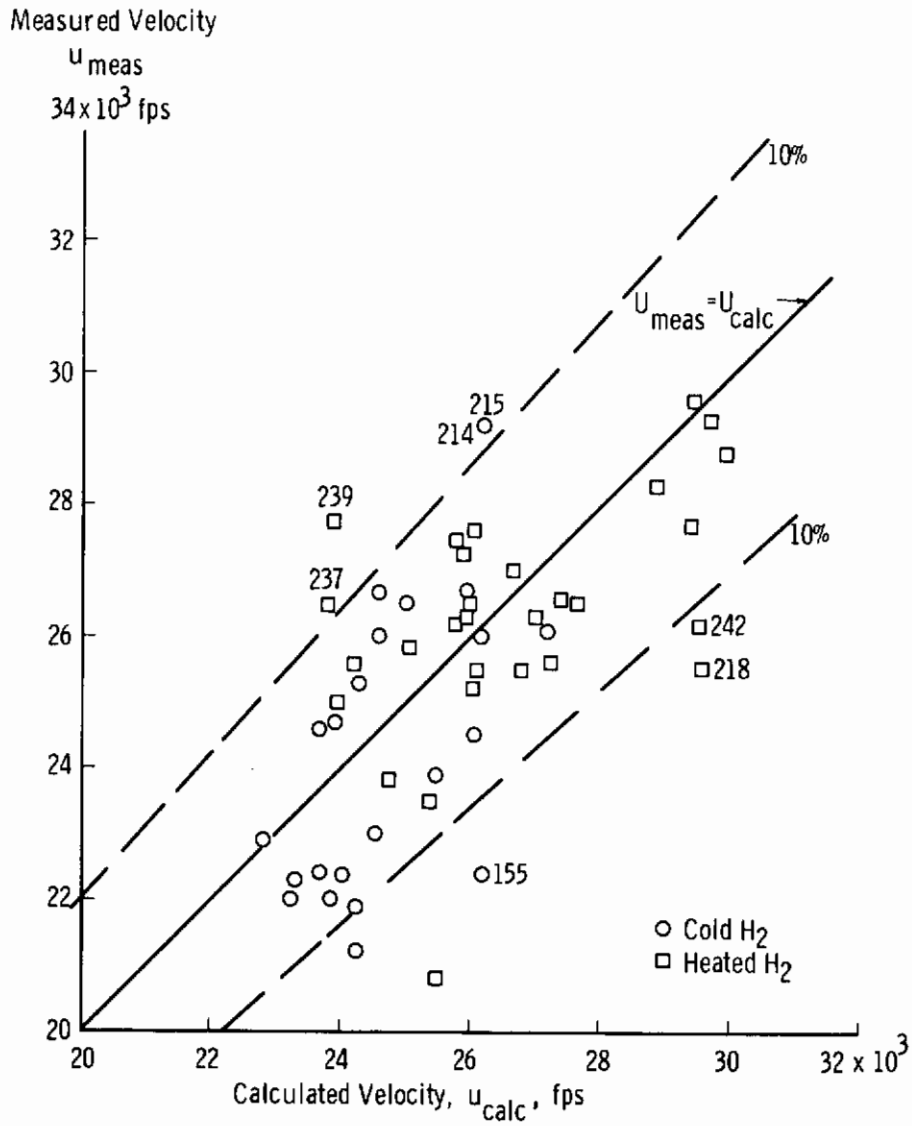

Fig. 12 Correlation of Experimental and Calculated Launch Velocity

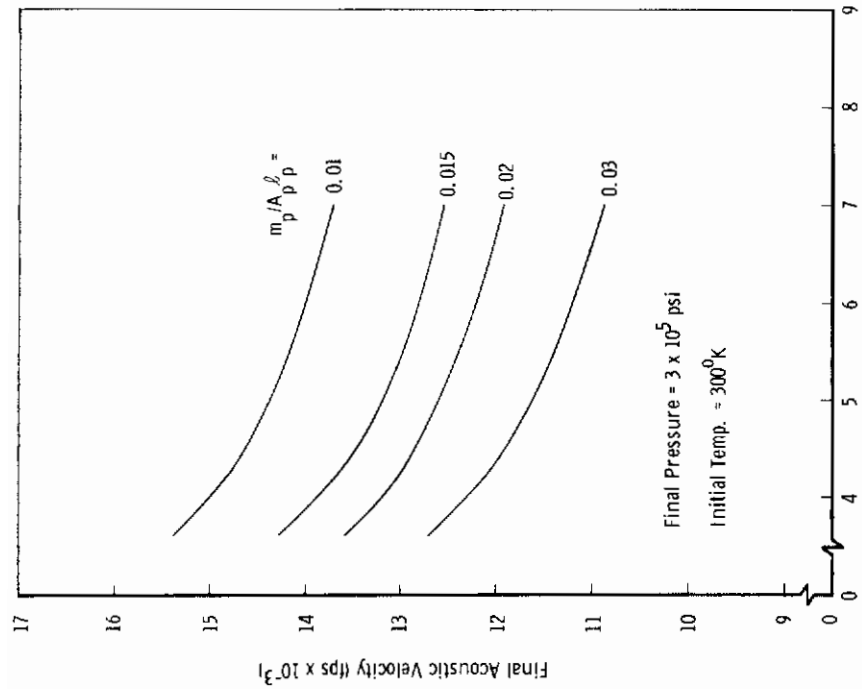

Fig. 14 Final Acoustic Speed in Pump Tube

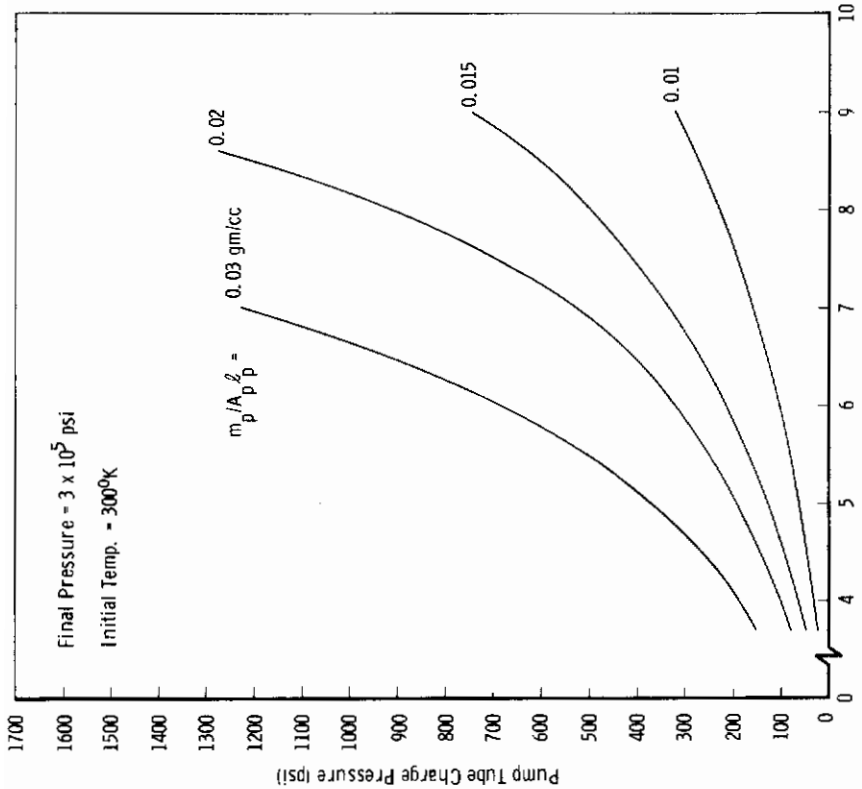

Fig. 13 Initial Charge Pressure for 3 x 10^5 psi Final Pressure

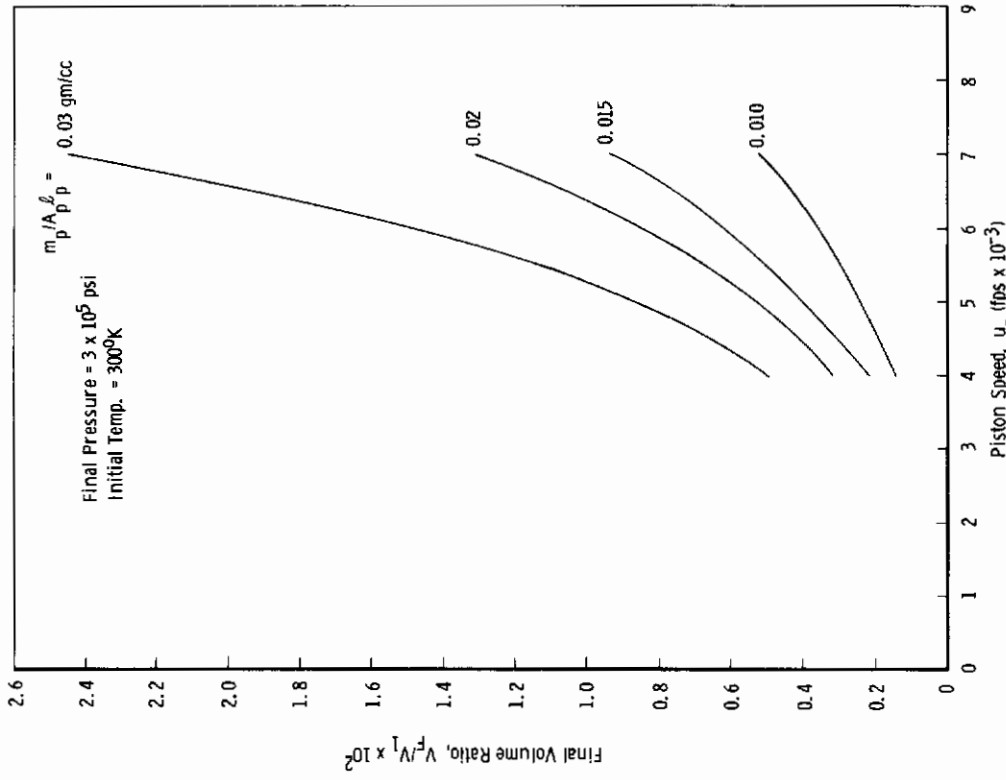

Fig. 15 Final Volume Ratio

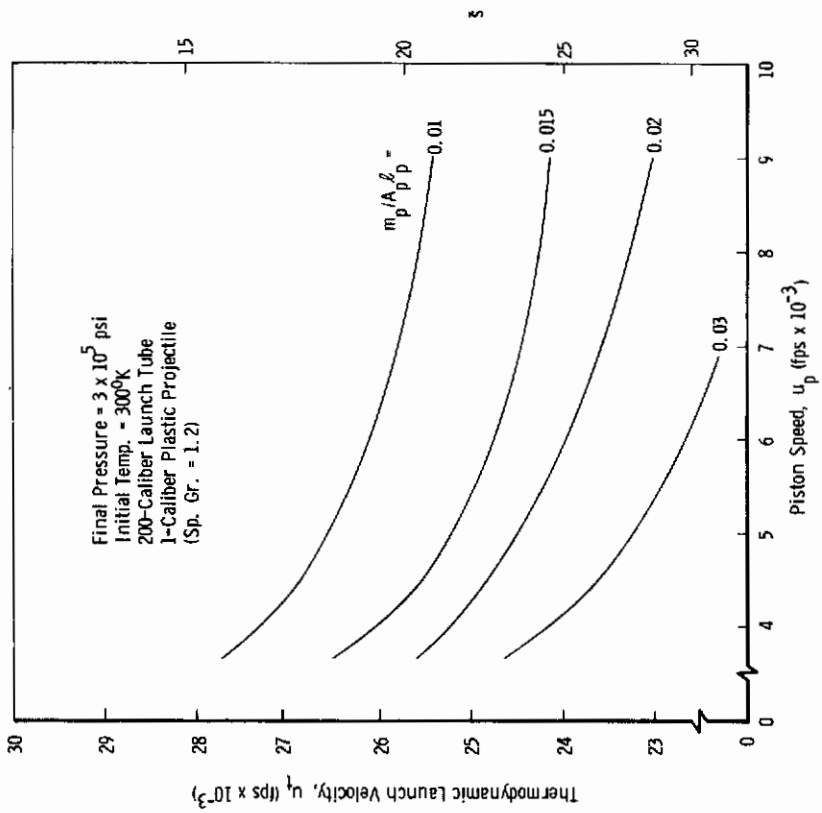

Fig. 16 Thermodynamic Launch Velocity for a 200-Caliber Launch Tube

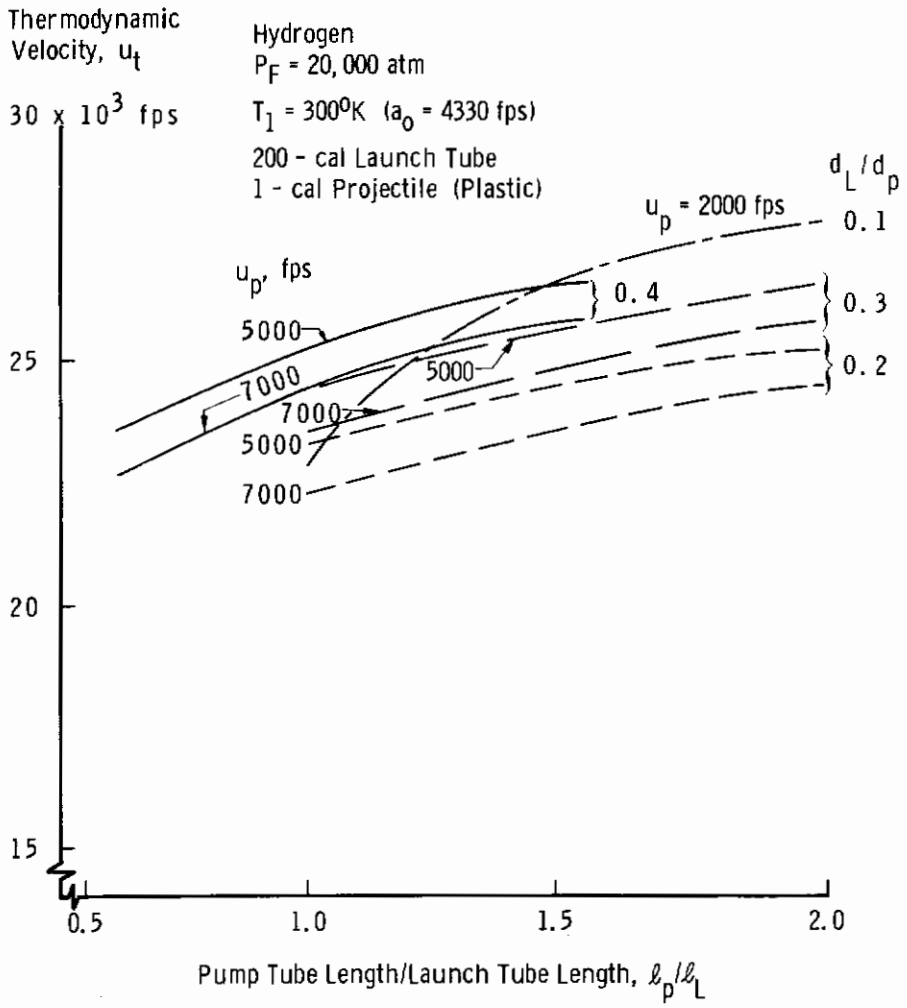

a. Thermodynamic Launch Velocity

Fig. 17 Effect of Launcher Geometry

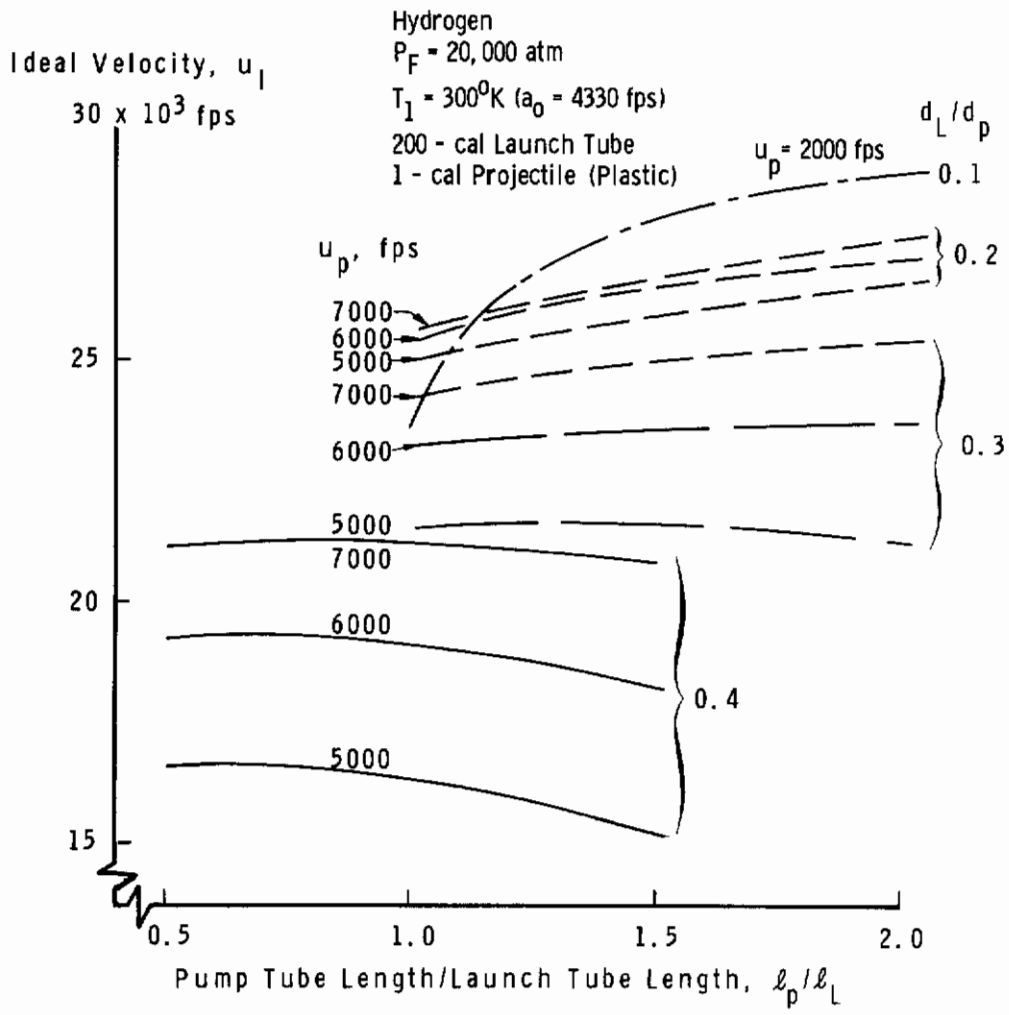

b. Ideal Launch Velocity

Fig. 17 Continued

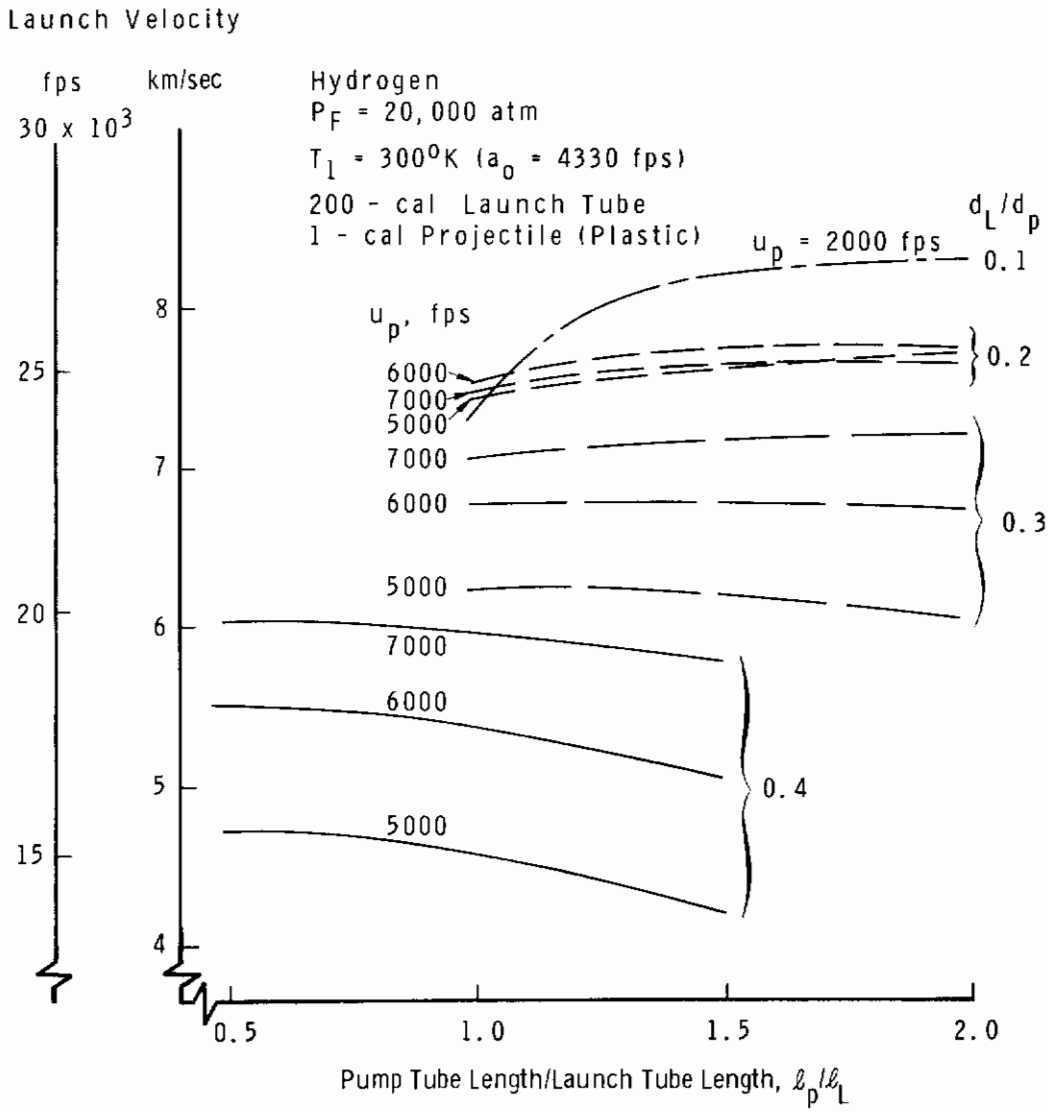

c. Corrected Launch Velocity

Fig. 17 Concluded

APPENDIX A
THERMODYNAMIC PROPERTIES OF HYDROGEN

In order to compute launch velocities, using hydrogen as the pump tube gas, the thermodynamic properties of the gas must be known throughout the range of gun operating conditions. Since only a limited amount of data was available (Refs. 7, 8, and 9) in the range of temperatures from 300 to 3000°K and pressures to 20,000 atm, a computer program was developed to bridge the gap between the two sets of data, and thus permit extrapolation of these data to higher pressures.

With the data prepared by Woolley, Hilsenrath, et al (Refs. 7, 8, and 9) and the empirical relationship*

$$Z = 1.000 + \lambda P$$

where

$$\log \lambda = a T + b$$

values of λ were calculated and plotted against temperature. This plot provided the constants:

$$a = -8.347 \times 10^{-4} \quad \text{and} \quad b = -2.9729$$

With the compressibility factor (Z) determined as a function of T and P, it was then possible to compute the enthalpy, entropy, and internal energy using relationships from Bridgman's tables as follows:

$$\left(\frac{\partial H}{\partial P}\right)_T = V - T \left(\frac{\partial V}{\partial T}\right)_P$$

where

$$V = \frac{Z R T}{P} = \frac{R}{P} Z T$$

and

$$\left(\frac{\partial V}{\partial T}\right)_P = \frac{R}{P}\left[Z + T \left(\frac{\partial Z}{\partial T}\right)_P\right]$$

then

$$\left(\frac{\partial H}{\partial P}\right)_T = V - \frac{RT}{P}\left[Z + T \left(\frac{\partial Z}{\partial T}\right)_P\right]$$

$$= V - \frac{Z R T}{P} - \frac{R T^2}{P} \left(\frac{\partial Z}{\partial T}\right)_P$$

*Suggested by Dr. M. Grabau of the Hypervelocity Branch, VKF.

Therefore

$$\left(\frac{\partial H}{\partial P}\right)_T = -\frac{RT^2}{P}\left(\frac{\partial Z}{\partial T}\right)_P$$

where

$$Z = 1 + [\log^{-1}(aT + b)]P = 1 + \{\exp[2.30259(aT + b)]\}P$$

$$\left(\frac{\partial Z}{\partial T}\right)_P = 2.30259\ aP\ \exp[2.30259(aT + b)]$$

$$\left(\frac{\partial H}{\partial P}\right)_T = -2.30259\ aRT^2\ \exp[2.30259(aT + b)]$$

at constant T

$$dH = \{-2.30259\ aRT^2\ \exp[2.30259(aT + b)]\}dP$$

$$H = H_o + \int_{P_o}^{P} -2.30259\ aRT^2\{\exp[2.30259(aT + b)]\}dP$$

$$\frac{H}{RT} = \frac{H_o}{RT} - 2.30259\ aT\{\exp[2.30259(aT + b)]\}(P - P_o)$$

Again from Bridgman's tables

$$\left(\frac{\partial S}{\partial P}\right)_T = -\frac{RT}{P}\left(\frac{\partial Z}{\partial T}\right)_P - \frac{RZ}{P}$$

as before

$$\left(\frac{\partial Z}{\partial T}\right)_P = 2.30259\ aP\ \exp[2.30259(aT + b)]$$

then

$$\left(\frac{\partial S}{\partial P}\right)_T = \frac{-RT}{P}\{2.30259\ a\ P\ \exp[2.30259(aT + b)]\} - \frac{RZ}{P}$$

at constant T

$$dS = \left\{-2.3026\ aRT\ \exp[2.3026(aT + b)] - \frac{RZ}{P}\right\}dP$$

$$S = S_o + \int_{P_o}^{P}\left\{-2.3026\ aRT\ \exp[2.3026(aT + b)] - \frac{RZ}{P}\right\}dP$$

$$\frac{S}{R} = \frac{S_o}{R} + \int_{P_o}^{P} -2.3026\ aT\{\exp[2.3026(aT + b)]\}dP - \int_{P_o}^{P}\frac{Z}{P}\,dP$$

where

$$\int_{P_o}^{P}\frac{Z}{P}\,dP = \int_{P_o}^{P}\frac{1 + P\exp[2.3026(aT + b)]}{P}dP$$

$$= \int_{P_o}^{P}\frac{dP}{P} + \int_{P_o}^{P}\exp[2.3026(aT + b)]\,dP$$

therefore

$$\frac{S}{R} = \frac{S_o}{R} - 2.30259\ a\,T\,(P - P_o)\ \exp\left[2.30259\,(a\,T + b)\right] - \ln\frac{P}{P_o}$$

$$- (P - P_o)\ \exp\left[2.30259\,(a\,T + b)\right]$$

$$\frac{S}{R} = \frac{S_o}{R} - (2.30259\ a\,T + 1)(P - P_o)\ \exp\left[2.30259\,(a\,T + b)\right] - \ln\frac{P}{P_o}$$

The internal energy (E) was calculated using the relationship

$$E/RT = H/RT - Z$$

and the density from the equation

$$\rho = P/ZRT$$

In these calculations where an initial value for the density was selected, the pressure was calculated by means of the equation

$$P = \frac{\rho R T}{1 - \lambda \rho R T}$$

The calculation procedure was then programmed for the IBM 7070 for selected values of initial pressure and temperature and also for values of initial densities and temperatures.

Figure A-1 shows the approximate ranges of the available data and present calculations. These computed values were then used to fair the region between the NBS data. Good agreement was obtained with NBS data in the 300 to 600°K range and also from 2200 to 3000°K. The computed values were used to a maximum pressure of 1000 atm, at which point the divergence from NBS data approached ten percent.

Reference 10 covers the range of density from 0.1 to 1000 Amagats and temperatures from 300 to 1200°K. Good agreement is obtained within the limits shown with the exception of the low temperature, high pressure region where Bjork's neglect of the co-volume effects causes a divergence.

With these data to fill the gap between the two sets of NBS data, it was possible to construct a Mollier Diagram (Fig. A-2). These results were then extrapolated to 100,000 atm to cover the operating range of interest for light-gas gun propellants. Figure A-3 gives internal energy, and Fig. A-4 shows the variation of acoustic velocity ($a = \sqrt{\gamma RTZ}$) deduced from the preceding data.

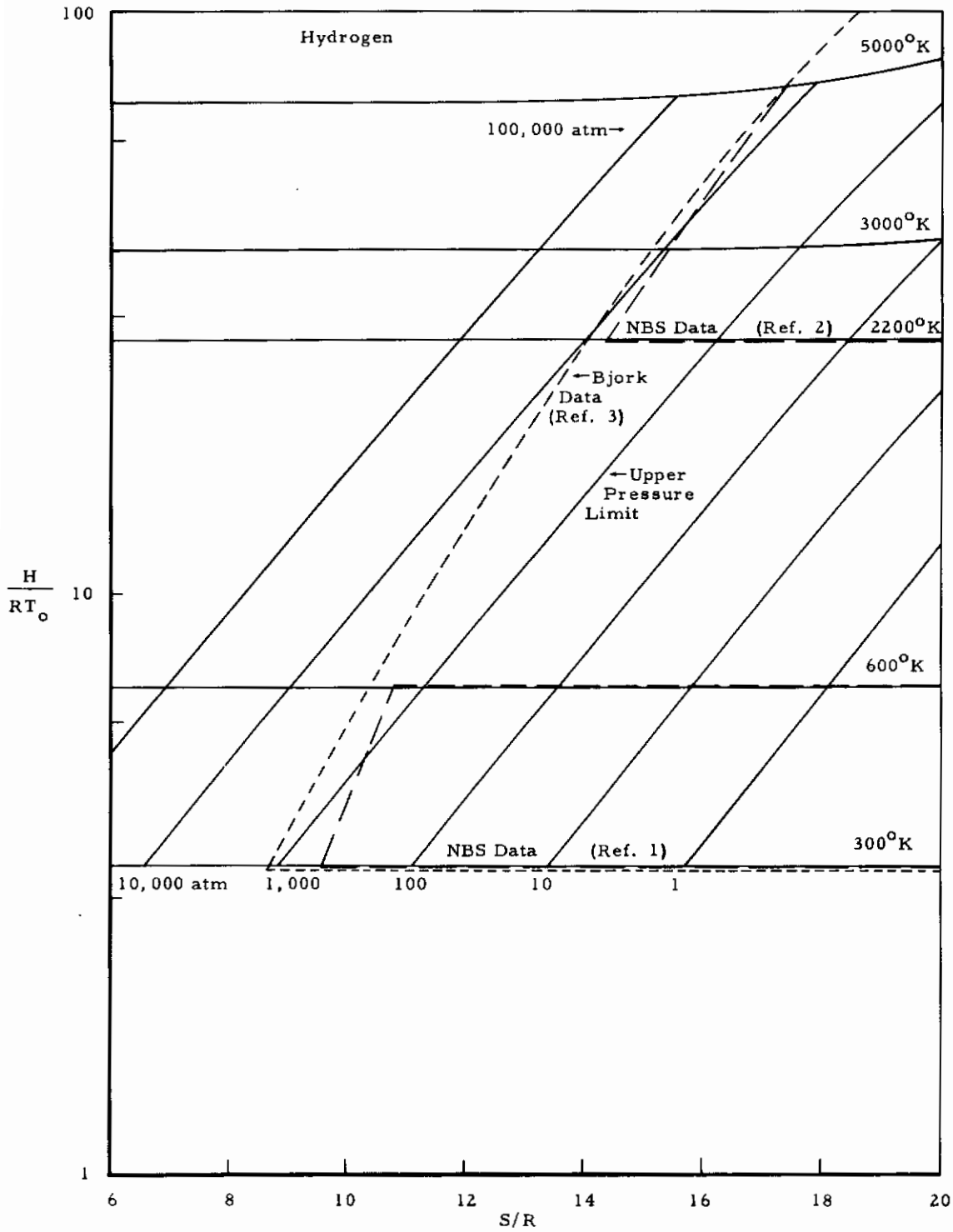

Fig. A-1 Limits of Applicability of the Empirical Equation

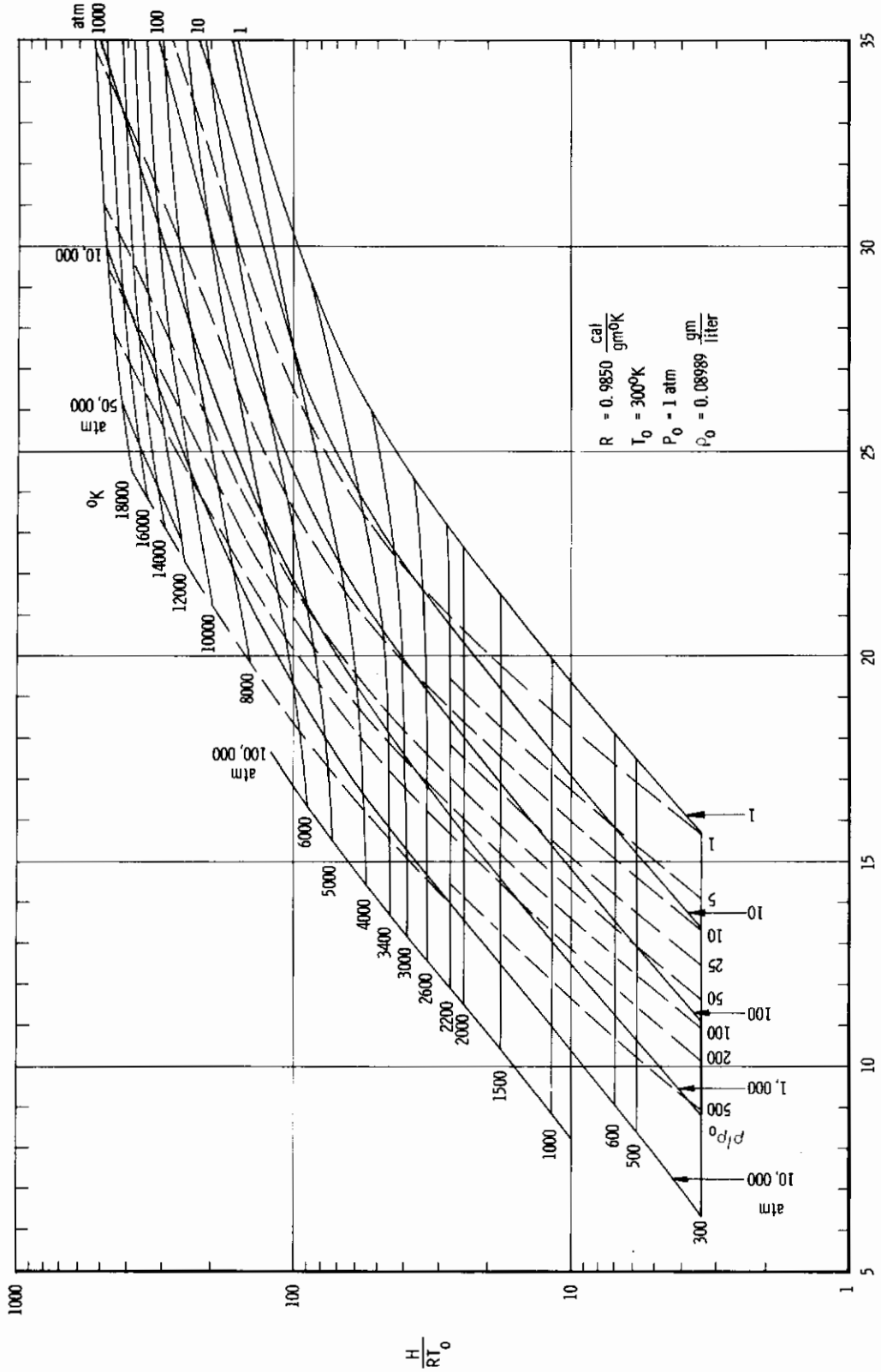

Fig. A-2 Mollier Diagram for Hydrogen

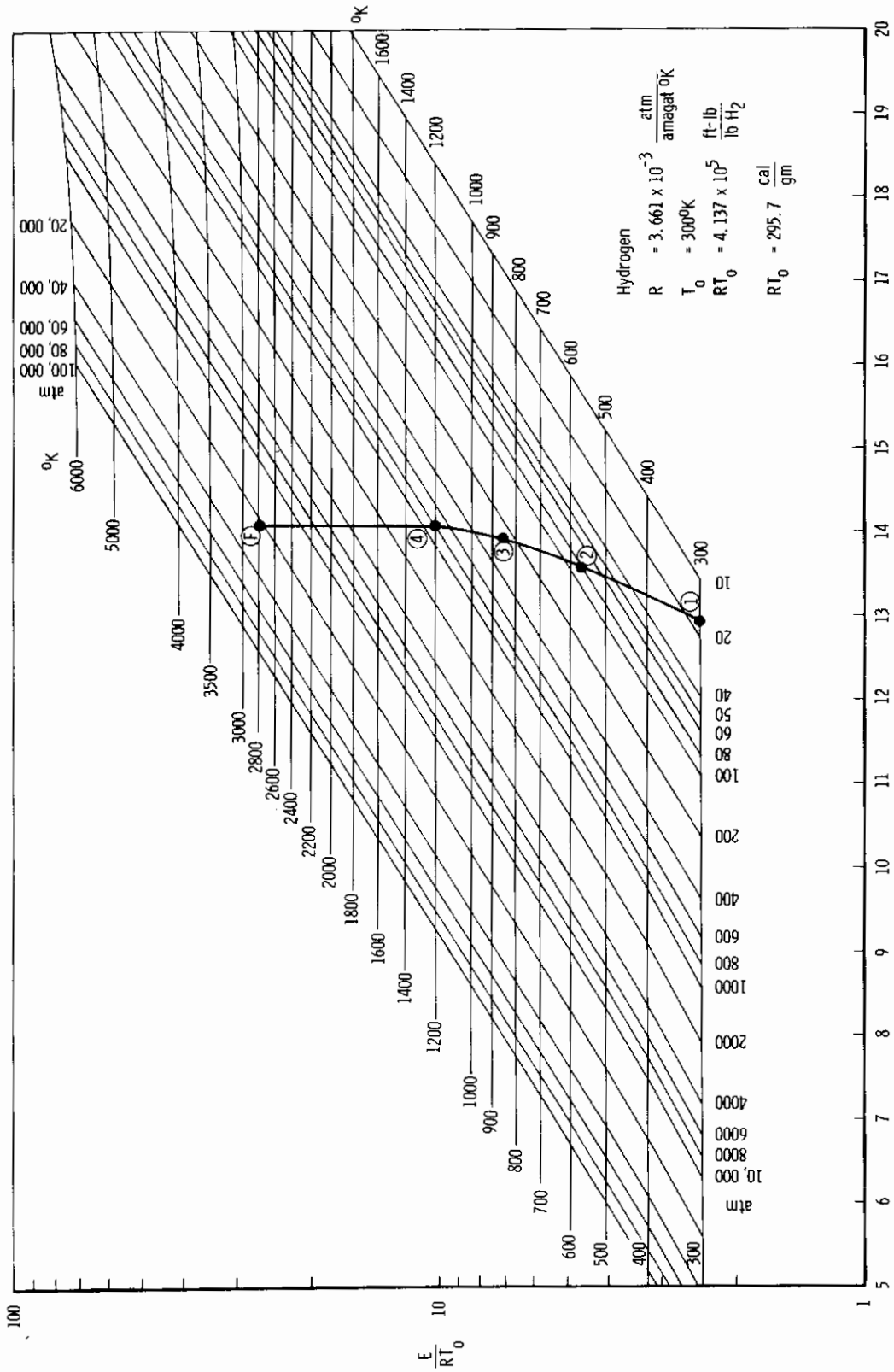

Fig. A-3 Internal Energy-Entropy Diagram

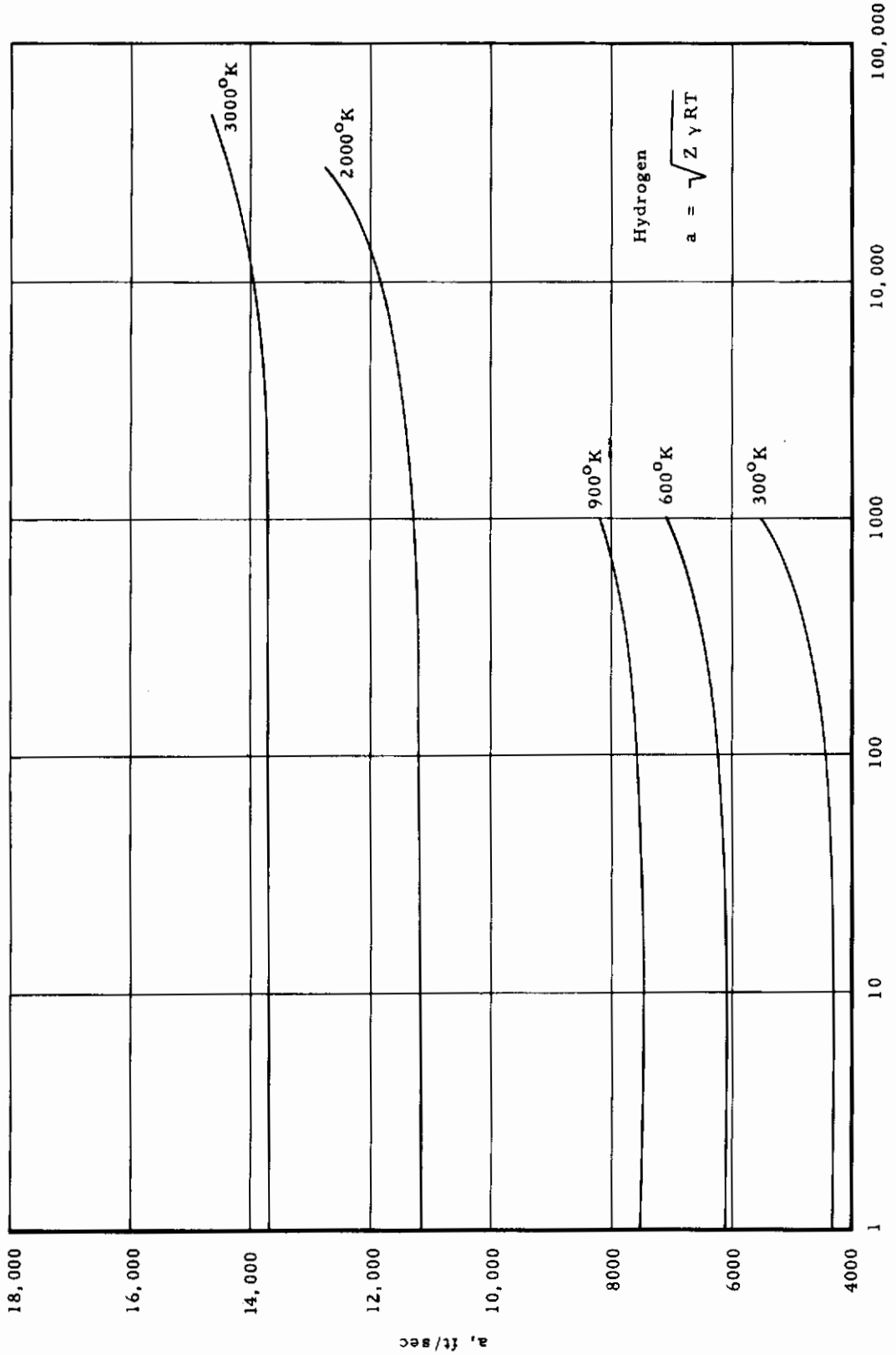

Fig. A-4 Acoustic Speed

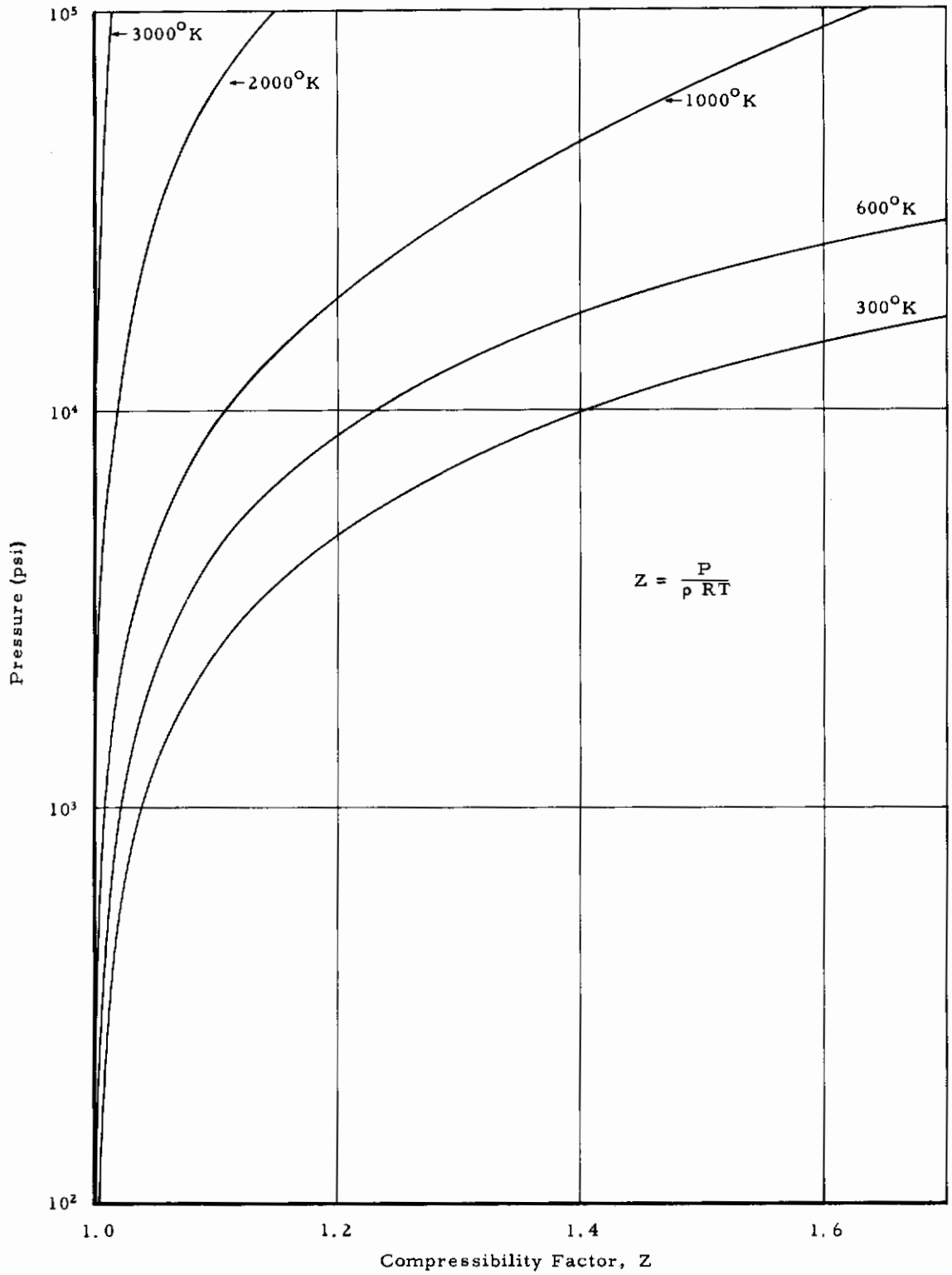

Fig. A-5 Compressibility Factor

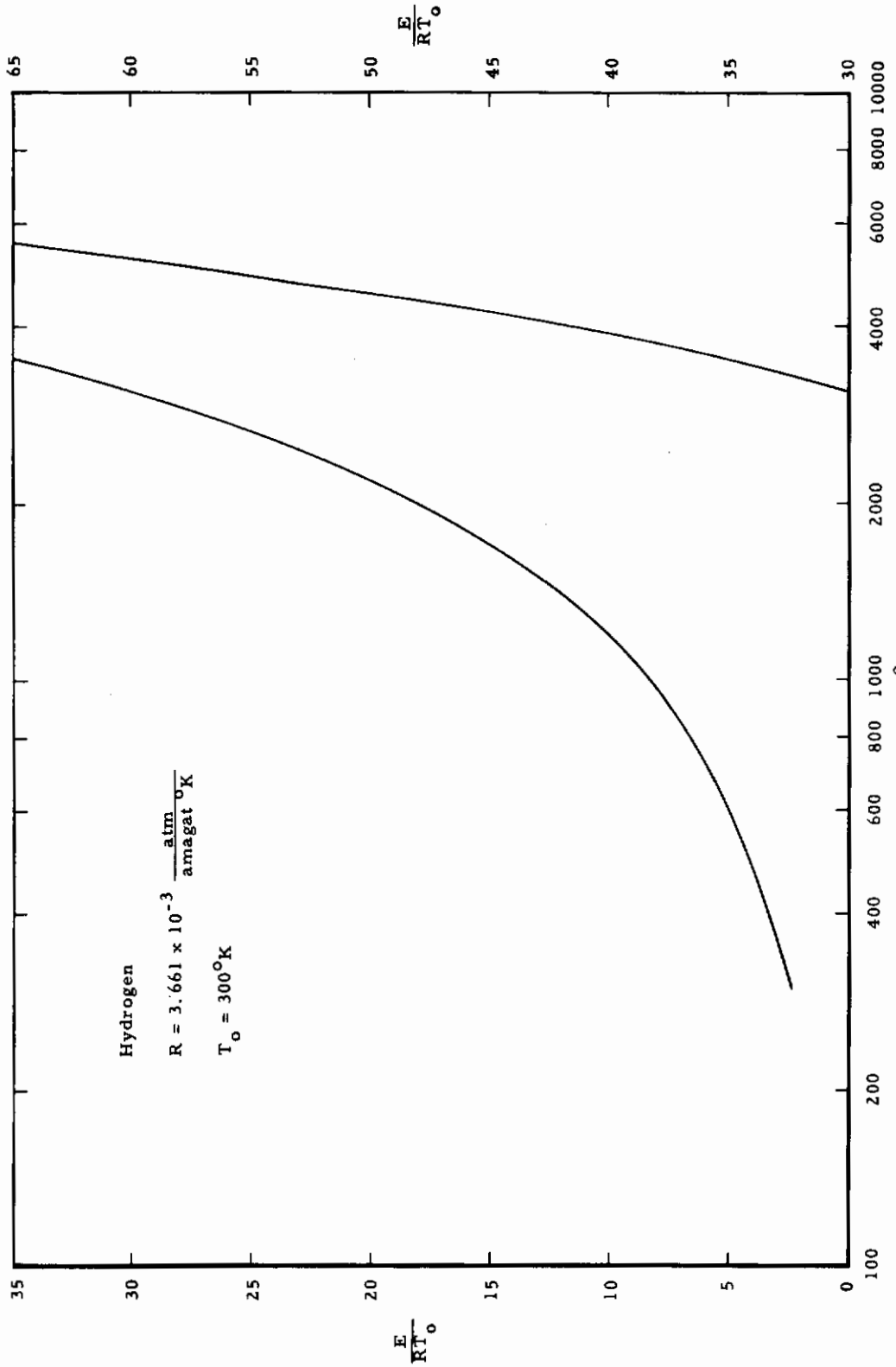

Fig. A-6 Internal Energy-Temperature Diagram

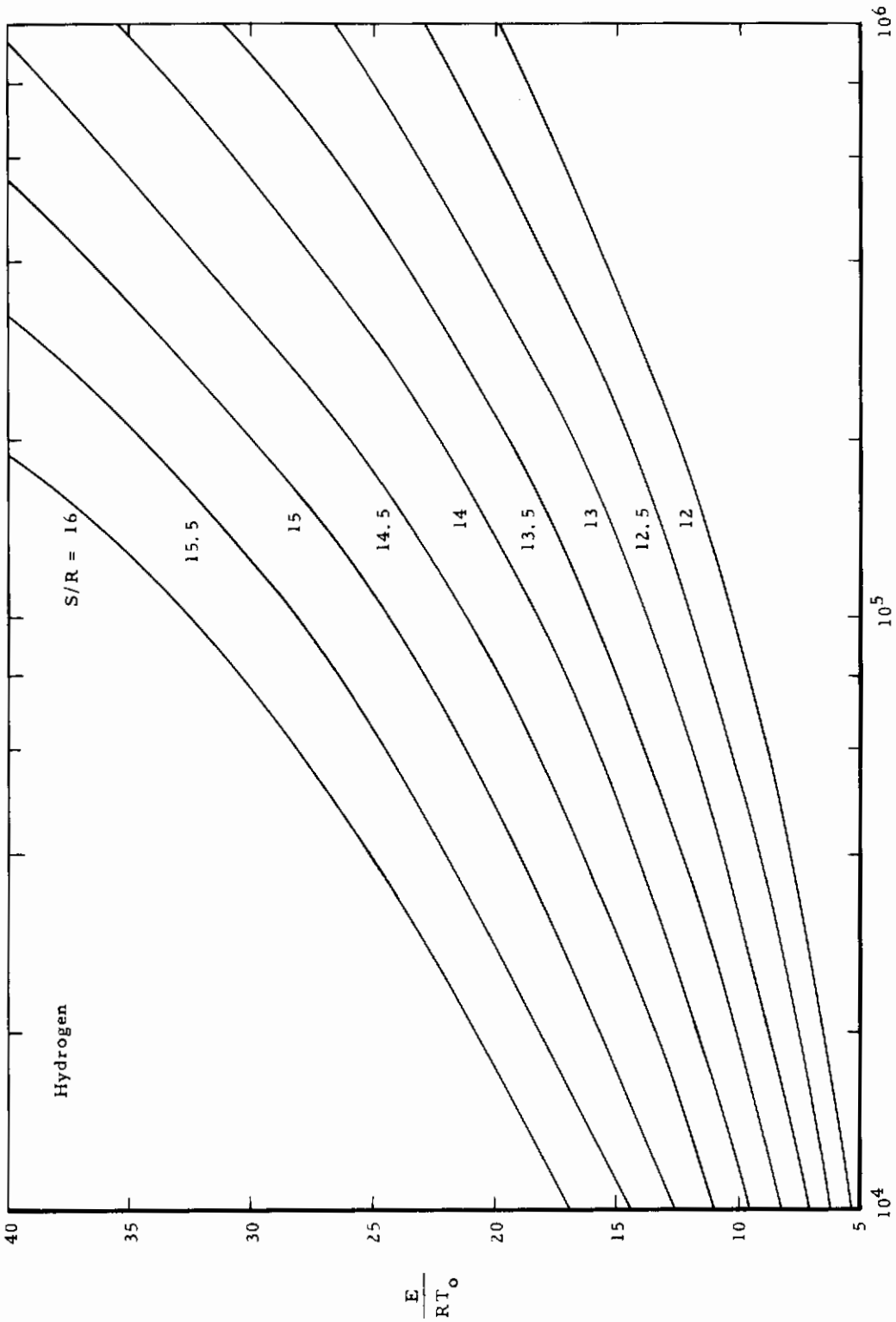

Fig. A-7 Internal Energy-Pressure Diagram

APPENDIX B

NORMAL SHOCK RELATIONS

The normal shock relations for hydrogen, treated as a real gas, are not available. Therefore, the graphical method outlined by Stollery and Maull (Ref. 11) was used to compute them.

By applying the energy, momentum and continuity equations to a stationary normal shock, we have:

$$H_1 + 1/2\ q_1^2 = H_2 + 1/2\ q_2^2$$

$$P_1 + \rho_1\ q_1^2 = P_2 + \rho_2\ q_2^2$$

$$\rho_1\ q_1 = \rho_2\ q_2$$

The conditions across a moving shock may be found by superposition of velocities:

$q_1 = u_S$ $\qquad$ u_S = Shock speed

$q_2 = u_S - u_p$ $\qquad$ u_p = Piston speed

Therefore

$$H_2 - H_1 = 1/2\ u_p^2 \left(\frac{\rho_2 + \rho_1}{\rho_2 - \rho_1}\right)$$

$$P_2 - P_1 = u_p^2 \left(\frac{\rho_2\ \rho_1}{\rho_2 - \rho_1}\right)$$

Which, in a general form for any further shock reflections, are:

$$H_{n+1} - H_n = 1/2\ u_p^2 \left(\frac{\rho_{n+1} + \rho_n}{\rho_{n+1} - \rho_n}\right)$$

$$P_{n+1} - P_n = u_p^2 \left(\frac{\rho_{n+1}\ \rho_n}{\rho_{n+1} - \rho_n}\right)$$

With the calculated piston velocity and the initial conditions in the pump tube, the initial shock Mach number can be found. With the shock Mach number and initial conditions determined, several values of ρ_2 are selected, and the corresponding values of H_2 and P_2 are calculated and plotted on the Mollier diagram. The point where the P_2 vs ρ_2 curve intersects the H_2 vs ρ_2 curve is the value of P_2 and H_2 behind the first shock. These values are then used as the initial conditions and the values behind the next shock computed.

This method was tried using the Mollier diagram constructed from NBS and computed data. The intersections were difficult to resolve on this plot, and therefore the data were replotted in the form shown below which proved to be superior in practice (Fig. B-1).

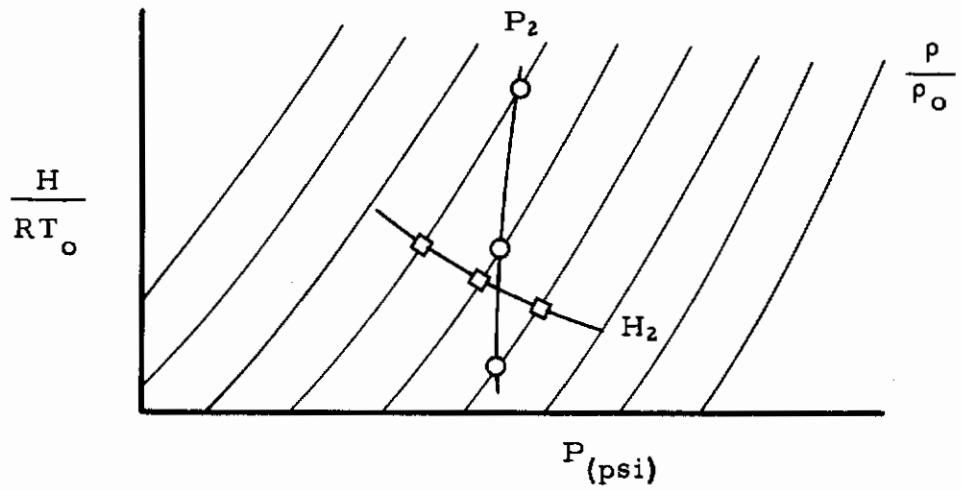

Fig. B-1 Enthalpy-Pressure Diagram

This plot gave better intersections and was easier to use than the standard Mollier diagram. The calculations were carried out for three shock passages (Figs. B-2a and b).

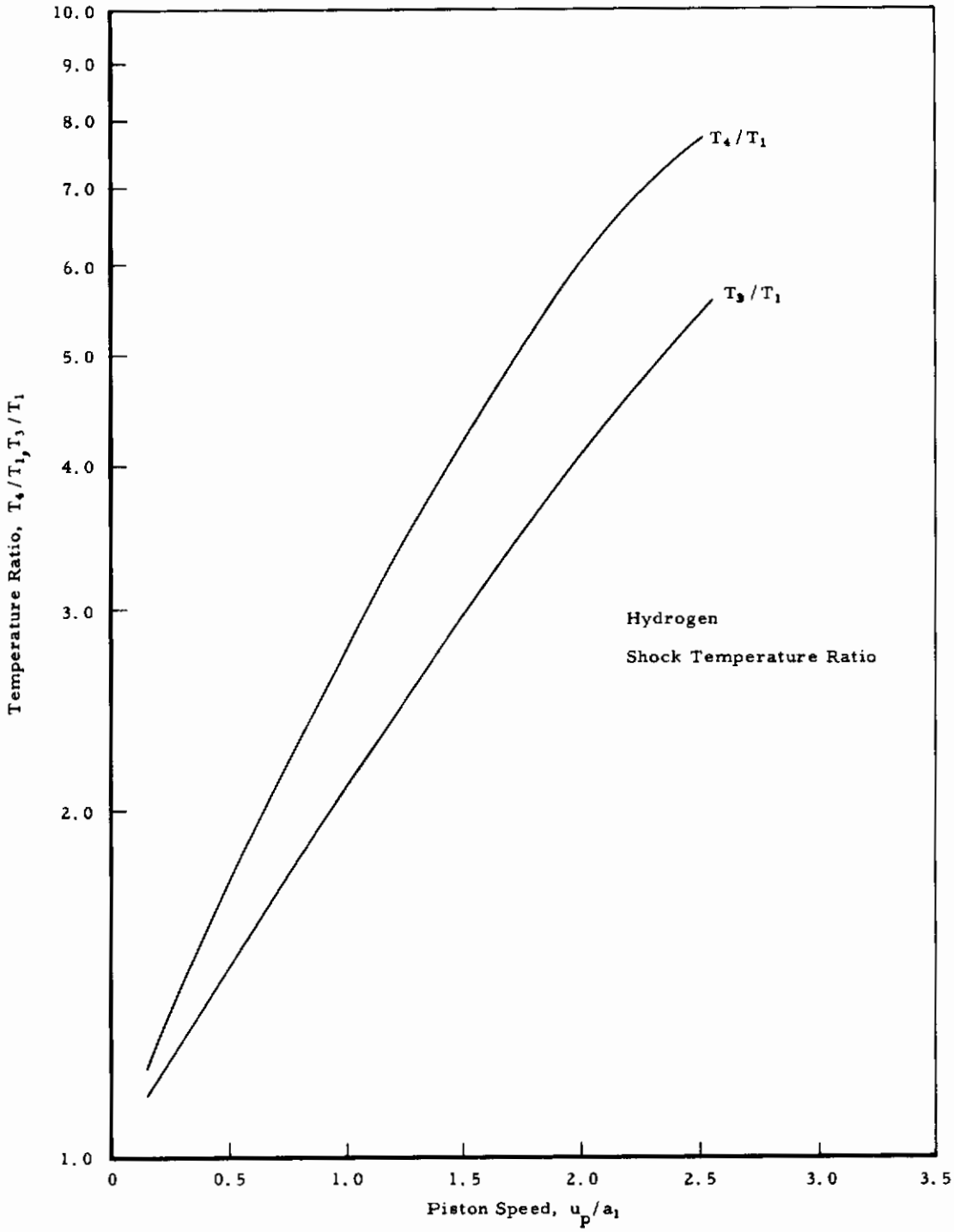

a. Temperature

Fig. B-2 Normal Shock Relationships

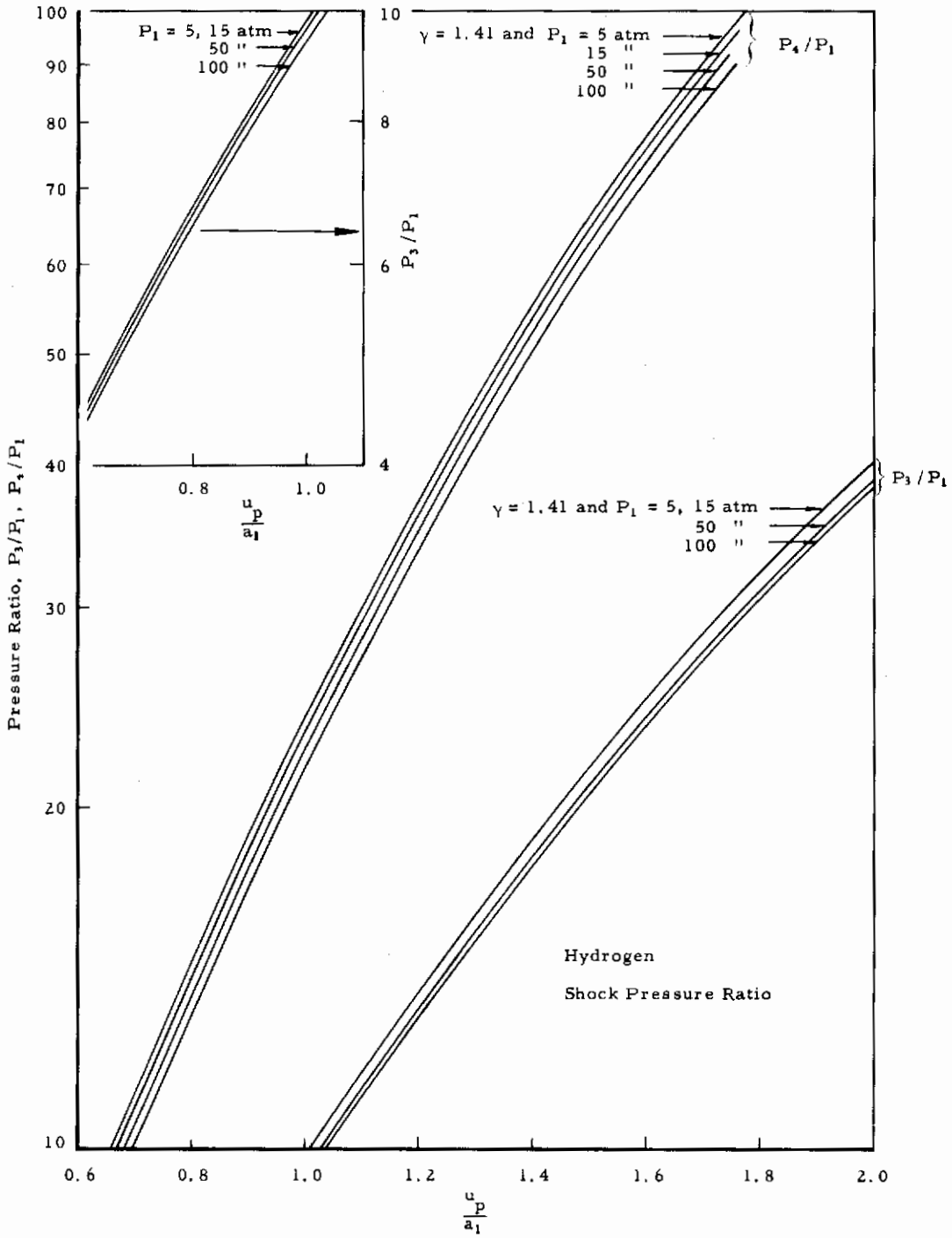

b. Pressure

Fig. B-2 Concluded